Mineralium Deposita (2021) 56:1111–1132
https://doi.org/10.1007/s00126-021-01044-5

ARTICLE

Chromitites of the Kraka ophiolite (South Urals, Russia): geological, mineralogical and structural features

Dmitry E. Saveliev[1]

Received: 3 October 2018 / Accepted: 20 January 2021 / Published online: 21 February 2021

Abstract

The paper describes disseminated tabular, podiform massive, and transitional chromitite deposits from a mantle section of the Kraka ophiolite massif, South Urals, Russia. The chromitite is hosted by dunite with no correlation between their size and quality and the size of the dunite bodies. Thick dunite bodies mostly host disseminated fine-grained banded chromitite; massive ores are composed of coarse-grained chromitite typically with a thin dunite envelope. The chromitite and host ultramafic rocks exhibit plastic deformation of silicates and chromite, which is expressed in microstructural features, preferred orientation of rock-forming olivine, and folding of the chromitite bodies. The ultramafic rocks are also characterized by deformation-induced textures leading to the formation of the small-size chromite grains on structural defects of plastically deformed rock-forming olivine and orthopyroxene. The formation of dunite bodies and associated chromitite is related to the localization of deformation of rising mantle flows under decompression conditions. Dunite was the most rheologically weak zone exhibiting a focused solid state flow and effective separation of mineral phases (olivine and chromite). The higher amount of the latter in dunite is a result of deformation-induced breakdown of enstatite and removal of trace elements from olivine. The structural features of massive chromitite aggregates indicate that they are a product of concentration and aggregation of grains under the influence of tectonic stresses at high temperatures and pressures, similar to pressure sintering.

Keywords Ultramafic rock · Chromitite · Cr-spinel · Olivine · Enstatite · Plastic deformation · Kraka ophiolite massif · South Urals · Russia

Introduction

The Urals is a fold belt with abundant ophiolite ultramafic massifs. The largest massifs (Voykar-Syn'ya, Kempirsay, Kraka, Ray-Iz, Syum-Keu) contain chromitite deposits of various productivity. For example, the Kempirsay massif in the South Urals hosts the world largest chromitite deposits in ophiolites: Almaz-Zhemchuzhina, Voskhod, Molodezhnoe, Komsomolskoe, and other deposits with reserves of up to 100 Mt of massive, metallurgical grade chromitite. The Ray-Iz massif in the Polar Urals hosts Tsentralnoe and Zapadnoe medium-sized deposits with reserves of up to 10 Mt of disseminated metallurgical chromitite. The Voykar-Syn'ya, Kraka, and Syum-Keu massifs contain only small-sized deposits and occurrences of chromitite. The Saranovskoe refractory chromitite deposit with reserves of 10 Mt of massive chromitite is hosted by a non-ophiolitic ultramafic–mafic complex in the western slope of the Central Urals (Fig. 1a).

The widely known lack of correlation between the size of ultramafic massifs and chromitite deposits still has no reasonable explanation. The formation of chromitite in ophiolite massifs is a matter of debate, which has been addressed in numerous publications (Rost 1959; Thayer 1964; Dickey 1975; Greenbaum 1977; Lago et al. 1982; Hock and Friedrich 1985; Leblanc and Ceuleneer 1992; Ballhaus 1998; Matveev and Ballhaus 2002; Borisova et al. 2012; Gonzalez-Jimenez et al. 2014; Arai and Miura 2016; Shiryaev and Vakhrusheva 2018; Zagrtdenov et al. 2018). Possible mechanisms of chromitite formation include crystal differentiation, liquid immiscibility, magma mixing, mantle/melt interaction, and solid state redistribution of mineral phases in a rising mantle flow.

The widely accepted melt-mantle interaction model is based on non-equilibrium between mantle melts and residual

Editorial handling: M. Fiorentini

✉ Dmitry E. Saveliev
savl71@mail.ru

[1] Laboratory of Ore Deposits, Institute of Geology — Subdivision of the Ufa Federal Research Centre of the Russian Academy of Sciences (IG UFRC RAS), Ufa, Russia

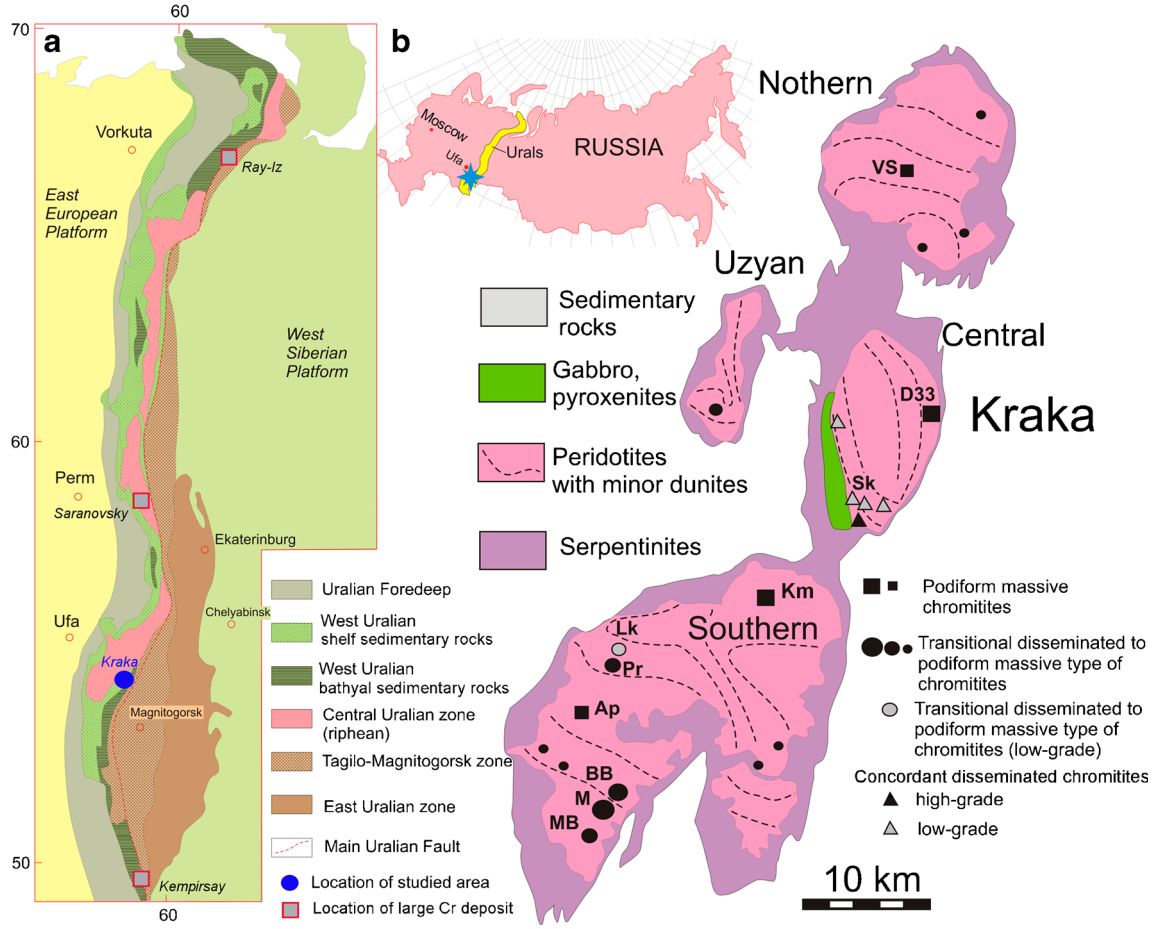

Fig. 1 Position of the Kraka ophiolite massifs within the Uralian fold belt (after Puchkov 1997) and their schematic geological map

peridotite, which therefore should have risen to the surface along isolated conduits, which are now ophiolitic dunite bodies (Kelemen et al. 1997; Spiegelman et al. 2001; Coccomazi et al. 2020). This model implies that percolating melts dissolve pyroxene and "crystallize" additional olivine finally leading to the formation of dunite. According to this concept, the formation of chromitite is considered to be related to boninite/peridotite interaction, dissolution of pyroxene, and crystallization of olivine and high-Cr spinel (Zhou et al. 1994, 1996, 2001). In contrast, we develop a rheomorphic model, which suggests the localization of plastic flow in the weakest layers (dunite) during the uplift of the mantle diapirs (Saveliev and Fedoseev 2014, 2019).

In spite of this conceptual diversity, there are grounds to believe that the final products of any ore-forming process reflect its evolution, i.e., the smallest chromitite bodies record the initial stages of the process, whereas the large and unique deposits correspond to advanced and final stages. Thus, the study of small chromitite deposits of the Kraka massifs may provide a key for favorable conditions for the formation of chromitite in dunite bodies.

Methods

The material for study was sampled by the author during field work in 1995–2018, which included geological and structural mapping and sampling of peridotite, dunite, and chromitite. The chromitite and rock samples were studied using traditional petrographic and precise analytical methods. Optical (as well as crystallographic) orientation of polycrystalline olivine aggregates is one of typical deformation features, which is studied in oriented thin sections on a universal stage (Fedorov's method). The thin sections were oriented relative to macroscopic structural elements of peridotite and dunite (e.g., foliation, lineation). Several polished sections 7 mm thick underwent oxidative thermal decoration (Kohlstedt et al. 1976) for 1 h at a temperature of 850 °C in order to reveal the dislocation structure of olivine.

Electron backscatter surface diffraction (EBSD) analysis was performed on a Hitachi S-3400N SEM equipped with an Oxford NordlysNano EBSD detector at Geomodel Resource Centre at an accelerating voltage of 30 kV, a beam current of 5 nA, and a beam focused to a point of no more than

100 nm (St. Petersburg State University, St. Petersburg, Russia).

The composition of minerals was analyzed on a SEM Vega 3 SBH Tescan equipped with an Oxford Instruments EDS X-Act at the Institute for Superplasticity of Metals, Russian Academy of Sciences (ISM RAS, Ufa, Russia) and Institute of Mineralogy, South Urals Federal Research Center of Mineralogy and Geoecology of the Urals Branch, Russian Academy of Sciences (IMin SU FRC MG UB RAS, Miass, Russia). The spectra were automatically processed using AzTec One software package and TrueQ technique. The SEM studies were conducted at an accelerating voltage of 20 kV, a current of 1 nA, a beam size of 3 μm, and an X-ray acquisition time of 60 s in spot-mode. The elemental compositions were quantified using standard samples of natural and synthetic compounds. The Fe^{2+} and Fe^{3+} contents of chromite were recalculated from stoichiometry.

The trace element composition of olivine was analyzed on an Agilent 7700x inductively coupled plasma mass spectrometer equipped with a New Wave Research UP-213 laser ablation system and MassHunter software package (D.A.Artemyev, IMin SU FRC MG UB RAS, Miass, Russia). Laser parameters: Nd: YAG UV, frequency quadrupled (wavelength of 213 nm), fluence 10–12 J/cm^2, pulse repetition frequency 10 Hz, ablation spot diameter 80–100 μm, pre-ablation 110 μm, carrier gas He, flow rate 0.6 l/min. Laser operation time: 5 s (pre-ablation) + 30s (background) + 60 s (analysis time). International glass standard reference materials were used for calculation, USGS GSD-1g and USGS BCR-2g. All mass fractions for USGS GSD-1g and USGS BCR-2g were taken from the GeoReM base preferred values (Jochum et al. 2005, 2011).

Geological setting

The Uralian fold belt consists of several longitudinal zones, which replace each other from the eastern margin of the East European Platform to the Mesozoic sedimentary cover of the West Siberian Platform, which overlaps the eastern part of the fold belt. According to Puchkov (1997, 2002), the structure of the Urals includes the following lithotectonic zones: Uralian Foredeep, West Uralian Zone, Central Uralian Zone, Tagil–Magnitogorsk Zone, and East Uralian Zone (Fig. 1a). The first three zones represent an ancient passive continental margin of the East European Platform and are separated from the paleoisland-arc complexes of the Tagil–Magnitogorsk Zone by the Main Uralian Fault suture.

Most ophiolite ultramafic rocks of the South Urals are serpentinized and are confined to the Main Uralian Fault Zone, Tagil–Magnitogorsk, and East Uralian zones with oceanic and island-arc rocks. Serpentinite forms small lenticular bodies in mélange zones.

The Kraka ultramafic massif, the largest massif in the Russian part of the South Urals, is located in the West Uralian Zone and has been moved to the present-day area from the Main Uralian Fault Zone (Kazantseva 1987; Puchkov 1997; Savelieva 1987). Senchenko (1976) and Saveliev et al. (2008) believe that it formed in the root part of an autonomous rift structure on a passive continental margin.

The Kraka ophiolite massif includes four blocks: Northern, Uzyan, Southern, and Central (Fig. 1b). The Northern, Uzyan, and Southern blocks are composed of peridotite with subordinate dunite. Significant amount of lherzolite and scarce dunite bodies occur in the Northern Kraka block. The Uzyan and Southern Kraka blocks are characterized by a banded dunite–harzburgite complex with ~ 10% of dunite. The Central Kraka block exhibits the most complex structure. Its central and eastern parts host spinel peridotite (lherzolite and diopside-bearing harzburgite) with rare and small veins of dunite and spinel–plagioclase peridotite. In the southwest, spinel peridotite grades into a dunite–harzburgite complex with dominant dunite. Further to the west, the complex consists of crustal wehrlite, clinopyroxenite, and gabbro.

Chromitite deposits and occurrences

All blocks of the Kraka massif host chromitite (Fig. 1b), which is most abundant in the southwestern part of the Central Kraka block (Saksey-Klyuchevskaya area) and the western part of the Southern Kraka block (Apshak and Bashart areas). According to structure and morphology (Cassard et al. 1981; Hock and Friedrich 1985), chromitite can be subdivided into three types: (1) mostly tabular disseminated bodies, (2) transitional from tabular disseminated to podiform massive chromitite, and (3) mostly massive podiform bodies. Relative to host peridotite, most ore bodies are concordant and, to a lesser extent, subconcordant. Chromitite is always hosted by dunite. Disseminated, fine-grained ores are typically enclosed in thick dunite bodies, whereas massive coarse-grained chromitite is often embedded into thin dunite envelopes.

The ore bodies show a large varieties in size and grade (Table 1). At the Shatran, Saksey, and Klyuchevskoe deposits, the resources were estimated for poorly disseminated chromitites with 5–15 wt.% Cr_2O_3.

Type 1 chromitite

The Saksey-Klyuchevskaya area occurs in the southwestern part of the Central Kraka block and includes several chromitite-bearing zones with tabular dunite bodies parallel to a mantle/crust boundary (paleo-Moho) and numerous small chromitite veins. Harzburgite is in graded contact with dunite.

Table 1 Chromitite deposits of the Kraka ophiolite massif

Deposits	Deposit type	Ore structures	Cr_2O_3 content of Cr-spinel, wt. %	Cr_2O_3 content of ore body, wt. %	Resources (promising resources), t	Period of exploitation
Menzhinsky	2	Densely and moderate-disseminated	60–63	25–45	200000	–
Bolshoy Bashart	2	Densely and moderate-disseminated, massive	60–63	30–45	30000	1860s–1930s; open pit
Maly Bashart	2		58–62	15–35	10000 (50000)	1930s, few open pits
No. 33	3	Massive, nodular	60–65	50–55	2000	2000s, open pit
Komintern	3	Densely disseminated, massive	?	30–40	1500	1930s, open pit
Saksey	1	Banded, disseminated	52–58	5–25	10000 (800000*)	–
Klyuchevskoe	1	Banded, poorly disseminated	52–56	5–15	– (1500000*)	–
Shatran	1		52–58	5–15	– (10000000*)	–
Pridorozhnoe	2	Banded, disseminated	58–65	10–30	5000 (20000)	2000s, open pit
Apshak area (dispersed ore bodies)	2	Banded, shlieren disseminated	47–58	15–35	5000 (20000)	1930s and 2000s, several pits
Verkhne-Saranginskoe	3	Densely disseminated, massive	52–58	35–45	500	1930s, pit
Chernaya Rechka	3	Densely disseminated	52-60	30–40	700	1930s, pit
Shigaevo	3	Densely disseminated, massive	52–58	30–40	500	1930s, pit
Occurrences	2–3	Densely and moderate-disseminated, massive	45–65	15–35	100–500	–

*estimated for 5–11 wt. % Cr_2O_3 on average

Transitional rocks contain a low amount of pyroxene. The area hosts the Saksey, Klyuchevskoe, and Shatran deposits of disseminated chromitite.

The Saksey deposit includes several (2–5) small chromitite veins within a thick dunite layer at the boundary between the mantle and crustal sections (Fig. 2a). The veins are few tens to hundreds meters long, several meters wide, and few centimeters to 2 m thick. The chromitite is characterized by NNW (330°) to NNE (10°) strike and almost vertical dip. Single thin clinopyroxenite veins cross cut the banded chromitite ores at angles of 10–30° and locally form networks (Fig. 2e, f). The locally folded and thickened chromitite bands form pockets, which are inclined at different angles to banding (Figs. 2b–d, h). Thin dunite veinlets also cut chromitite bands at different angles.

The Shatran deposit has a structure similar to the Saksey deposit, but is located in the mantle section 1 km below the paleo-Moho surface. It contains no clinopyroxenite veinlets in dunite and chromitite and is the largest deposit of disseminated chromitite with resources of 10 Mt of ore at 7 wt. % Cr_2O_3.

Type 1 chromitite mostly exhibits disseminated and rare massive structures. The evenly disseminated chromite is characterized by an equigranular texture (0.0 n–0.1 mm) with increasing grain size toward massive ores and heterogeneous grain distribution. The banded chromitite (Fig. 2b) consists of alternating ore and barren interlayers of poorly disseminated banded ores ranges from a few millimeters to 1–2 cm in thickness. With the increasing thickness of ore interlayers, chromitite exhibits gradual or sharp transition to host dunite with contrasting distribution of chromite. The most valuable densely disseminated and massive chromitite is subordinate at the deposits and forms interlayers within banded chromitite.

The ore bodies of this type deposits are characterized by specific "occluded silicate structure" (Fig. 2i–k), where numerous ovoid fragments of serpentinized olivine, with an average diameter of 2.5 cm and a width/length ratio of 1:2–1:5, are rimmed by chromite grains. The long axis of olivine aggregates is parallel to the banding in chromitite. The areas with this structure are often spatially juxtaposed with densely disseminated banded and nodular ores.

Chromite in these deposits exhibits a fine-grained texture and euhedral or subhedral grains with smooth contours, which may indicate solid state transportation. The grain size varies from a few micrometers to 1 mm and most grains are + 0.05–0.2 mm in size. The formation of aggregates from several

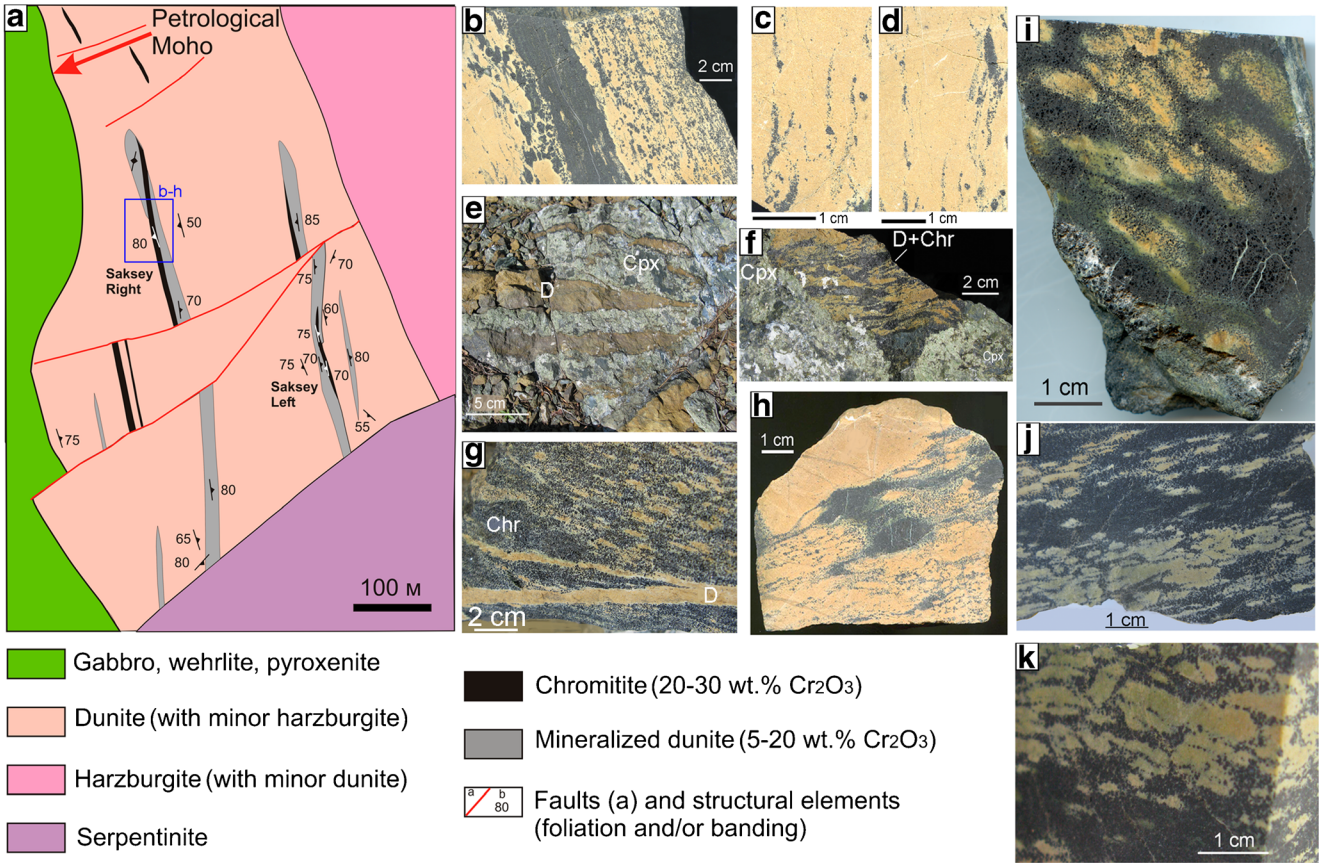

Fig. 2 **a** Geological map of the Saksey deposit. **b–h** Structural features of chromitite: **b** Banded texture of disseminated fine-grained chromitite. **c**, **d** Chromitite streams in dunite. **e**, **f** Clinopyroxenite veinlets in dunite and banded chromitite. **g** Dunite veinlets in densely disseminated chromitite. **h** Folded chromitite in dunite. **i–k** Occluded silicate texture in chromitite

closely adjacent chromite crystals leads to the increase in grain size and the formation of a system of transverse fractures similar to "pull-apart" structure (Fig. S1).

Type 2 chromitite

This type of chromitite includes the Menzhinsky, Bolshoy Bashart, and Maly Bashart deposits and occurrences of the Apshak area located in the western part of the Southern Kraka block (Fig. 3). The Bolshoy Bashart deposit is composed of several parallel veins grading to a branchy vein body. The veins are 0.5–2.5 m thick and are hosted by serpentinized dunite bodies up to 20 m thick. The dunite is surrounded by massive spinel peridotite with higher amount of enstatite (25–30 vol. %). The outcrops of spinel–plagioclase peridotite occur few tens meters above the ore bodies. The chromitite–dunite zone is almost horizontal and gently (10–15°) dips to the north. The chromitite is massive to densely disseminated and often exhibits deformation features including pull-apart structure, folding, boudinage of dunite within massive chromitite, boudinage of chromitite within dunite, and chromitite "snow-ball" textures. The olivine grains in dunite are deformed, which is typical of mantle tectonites (Nicolas 1989).

The Menzhinsky deposit includes several extended (~ 1000 m long) thin (0.3–1.5 m) chromitite bodies hosted by a flattened dunite lens 30–60 m thick. The contact between dunite and country rock peridotite is sharp. The peridotite contain up to 30 vol. % of enstatite. The dunite host harzburgite veinlets with 10–15 vol. % of ortopyroxene, which are concordant to dunite-chromitite banding. The concordant banding and foliation strike to the northwest and dip to the northeast at an angle of 45°. The chromitite is characterized by disseminated or massive structure.

The Maly Bashart deposit has similar structural features to the Menzhinsky deposit. Peridotite of the Maly Bashart deposit hosts an extended NW-trending dunite body (Fig. 3a). This body contains a series of parallel discontinuous veins of disseminated chromitite, which forms an ore zone generally concordant to contacts with dunite and pyroxene banding in country rock harzburgite.

The chromite-bearing zone is characterized by swells and pinches of a chromitite-bearing zone (Fig. 3b). The lenticular

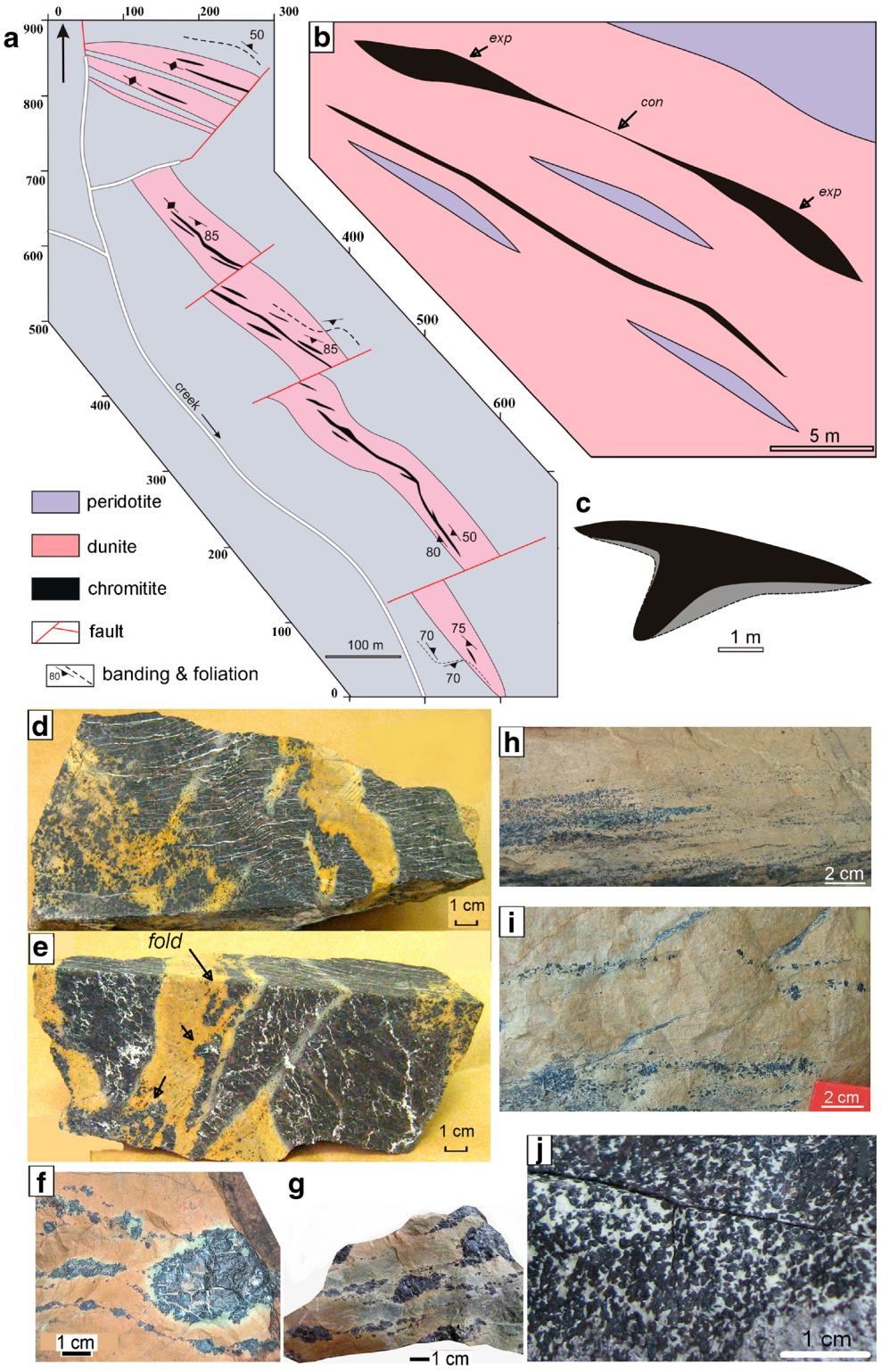

Fig. 3 **a** Geological map of the Maly Bashart deposit. **b** Schematic map of area no. 4 of the deposit. **c** Morphology of a typical ore body. **d–g** Structural features of chromitite of type 2 deposits: **d**, **e** Folded massive chromitite in dunite from the Pridorozhnoe deposit. **f**, **g** Boudinage of chromitite in dunite from the Bolshoy Bashart deposit. **h–i** Chromitite chains in the pinch out of the chromitite-bearing zone. **j** Nodular chromitite sampled near massive chromitite from the swell of the chromitite-bearing zone

and podiform massive to densely disseminated chromitite is located in swells (Fig. 3c) transiting to thin veinlets of moderately disseminated ore in pinches. The chromite-bearing zone is divided by a series of NE-trending strike-slip faults into five blocks 70–150 m long. In the southern part, the dunite body narrows and pinches out and grading to peridotite with high pyroxene amount (25–30 vol. %) is more striking than in the northern end of the zone. The chromitite bodies of

the deposit are 0.1–0.4 m thick; the densely disseminated chromitite with 30–40 wt. % Cr_2O_3 are dominant. The areas of poor chromite dissemination up to 1.5 m thick locally occur.

The Apshak area is situated in the western part of the South Kraka block, north of the Bolshoy Bashart and Menzhinsky deposits and includes the Laktybash and Pridorozhnoe deposits. They generally are similar to above deposits. The chromitite is disseminated, banded, fine- to medium-grained and contains 10 to 50 vol. % of chromite. The host rocks are completely serpentinized dunite. The chromitite-bearing zones are 100–200 m long; dunite is 50–100 and 20–40 m thick at the Laktybash and Pridorozhnoe deposits, respectively. The ore-bearing zones are 10–15 m thick and contain thin parallel chromitite streams (0.05–0.3 m) and ore banding strike to the WNW (270–300°) and vertically dip to the NNE (0–30°). The ore-bearing dunite locally contains veinlets and schlierens of peridotite. Foliation, chromitite banding, and lineation, which are emphasized by spinel chains, are concordant with each other in dunite and peridotite. The chromitite bands are often folded. Ore includes lenses of massive chromitite typical of the central part of the Pridorozhnoe deposit. Numerous massive chromitite lenses exhibit isoclinal folds with parallel axial planes (Fig. 3e). This feature is evidence of redistribution of mantle material during solid state flow.

Chromitite of the Menzhinsky and Maly Bashart deposits is characterized by banding, which is caused by chains of chromite grains (Figs. 3h, i) in alternance with variously disseminated and granular bands. Massive, spotted, and sparsely disseminated ores are rare. Various grain size is mostly typical of sparsely disseminated fine-grained chromitite (0.1–1 mm), in which the grain size consistently increases to medium- and densely disseminated and massive chromitite. The densely disseminated and massive chromitite often exhibits a combination of medium-grained and rare lenticular and schlieren coarse-grained aggregates (with grain size up to 1 cm).

The Bolshoy Bashart deposit contains dominantly massive to densely disseminated, and subordinate medium to sparsely disseminated chromitite with most common banded, abundant schlieren/spotted, and rare nodular structures with nodule sizes of 2–5 to 5–15 mm (Fig. 3j). Chromitite is characterized by abundant euhedral, coarse-grained (1–5 mm) and minor medium- (0.5–1 mm) to fine-grained (0.1–0.5 mm) chromite. Small grains frequently compose rare dissemination and are accessory in dunite.

Type 3 chromitite

Typical podiform deposits of the Kraka massifs are small but numerous (Fig. 4). The largest deposits contain few thousands of tons of chromitite (Komintern and no. 33 deposits). The subconcordant no. 33 deposit is situated in the eastern part of the Central Kraka block. The orebody 50 m long and 1.5–2 m thick is composed of massive chromitite surrounded by a thin (0.1–3.0 m) dunite envelope and is characterized by numerous swells and pinches. The nodular ores locally occur along the contact of massive chromitite and dunite. The contact between peridotite and dunite is sharp and the amount of pyroxene in peridotite increases up to 30–40 vol.% close to the contact. The ore zone of the deposit is extended in a longitudinal direction; the dip of chromitite and dunite contacts is almost vertical, whereas the plunge is horizontal. Thin dunite veinlets (few centimeters thick) with a shallow western dip at an angle of 15–30° intrude peridotite from the main dunite body.

These deposits exhibit abundant coarse-grained dense-disseminated, massive, and coarse-nodular ores (Fig. 5a–d). In particular, massive and nodular chromitite at the no. 33 deposit is composed of ~ 70% of the ore body. Sparsely disseminated fine-grained chromitite is minor. Massive chromitite exhibits strain-induced aggregates and interstitial silicates (Fig. 5e). In numerous samples, softer silicates (olivine, serpentine) are squeezed from intergranular space in chromitite to the outer zones (Fig. 5e, f). Massive chromitite is characterized by variously granular texture including extremely large anhedral crystals and smaller grains along their periphery.

In chromite aggregates, the grains are intergrown and their contacts become obscured indicating coalescence under high pressure and temperature. Progressive deformation generates new low-angle boundaries, which can be identified only by means of EBSD analysis (Fig. 5g, h). Adjacent chromite aggregates form along parallel straight boundaries, which can also be shifted along shear zones (Fig. 5f).

Composition of minerals

The major rock-forming minerals of the Kraka ultramafic rocks include olivine, orthopyroxene, and clinopyroxene, whereas chromian spinel is an accessory mineral. Orthopyroxene is characterized by high MgO content corresponding to enstatite. Mg–Ca clinopyroxene is diopside. The main trace elements of pyroxenes (Al and Cr) show a positive correlation in both ortho- and clinopyroxene (Fig. 6a–c). The composition of orthopyroxene depends on its morphology and size. Large porphyroclasts have the highest contents of Al_2O_3 (1.5–5.0 wt. %) and Cr_2O_3 (0.5–0.9 wt. %) in contrast to equiaxial neoblasts (< 2 wt. % Al_2O_3 and < 0.5 wt. % Cr_2O_3) (ESM-02).

The Fo amount of high-Mg olivine varies from 90% in lherzolite to 94–95% in dunite (ESM-02). The increase in Mg# value of olivine is accompanied by the increase in Cr content of coexisting Cr-spinel (Fig. 6d). Nickel (0.10–0.67 wt.% NiO) is a typical trace element of the Kraka olivine. The

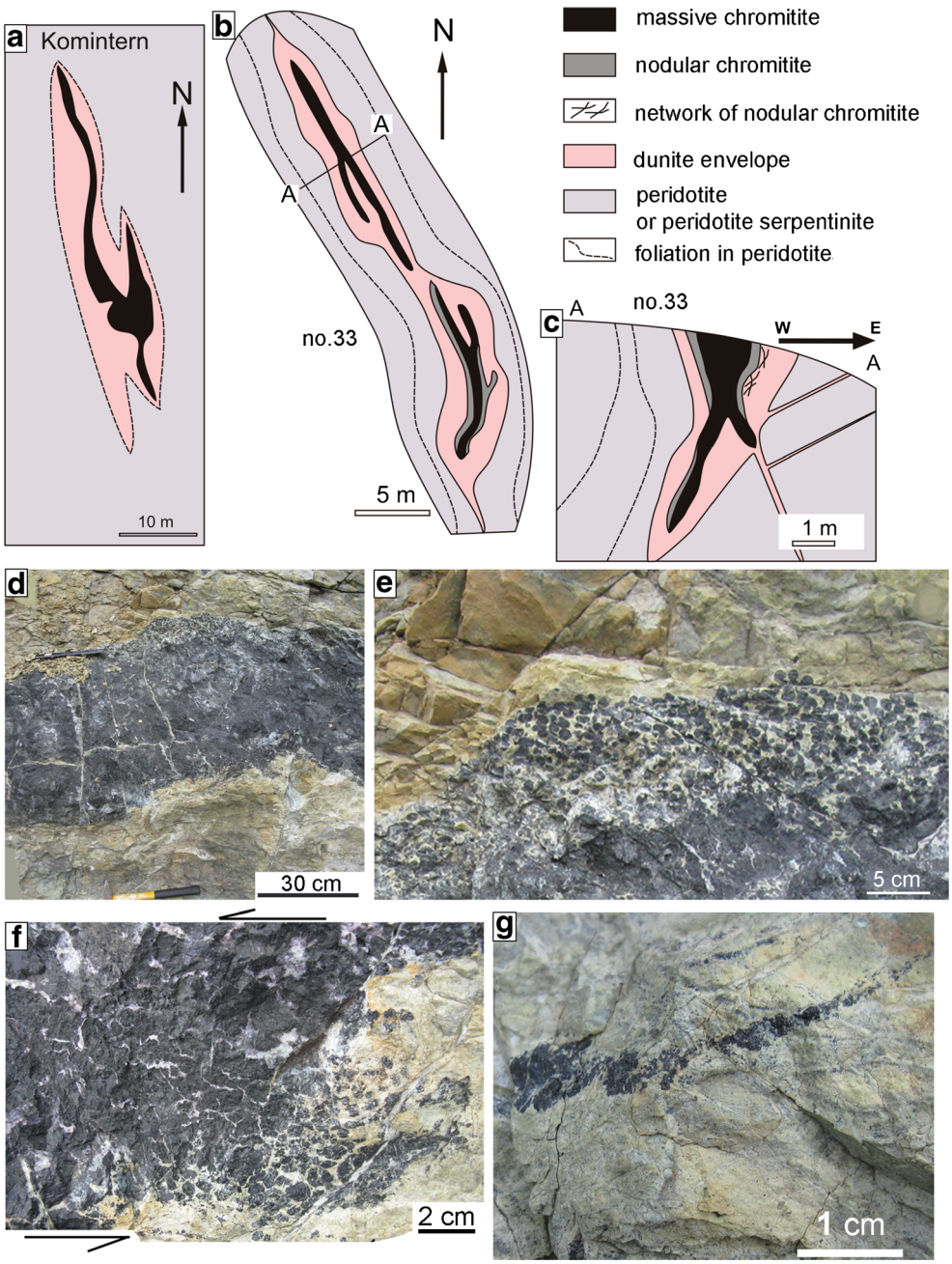

Fig. 4 **a**, **b** Geological maps of typical podiform Komintern deposit (**a**) and no 33 deposit (**b**). **c** Cross-section of the no 33 deposit. **d**–**g** Structural features of chromitite of the no 33 deposit: **d** Outcrop of massive chromitite ore body. **e**, **f** Nodular chromitite at the contact massive ore and dunite. **g** Folded chomitite in dunite

contents of other trace element contents are below detection limit. Some analyses contain minor MnO and CaO (up to 0.35 and 0.6 wt. %, respectively).

The chemical composition of the Kraka chromian spinel spans the entire compositional range typical of ophiolitic spinels. On ternary Al–Cr–Fe^{+3} diagram, data compositions form a continuous narrow trend from high-Al spinel in lherzolite to high-Cr spinel in dunite and chromitite (Fig. 6e–j). The Mg#–Cr# diagram (Fig. 6k) demonstrates more complex correlation, where the Al-rich spinel in lherzolite are Mg-rich and the Fe# value increases with increasing Cr/Al ratio, reaching its maximum in accessory Cr-spinel in dunite. Chromitite, however, exhibits an opposite trend with increasing Mg# and Cr# values or constant Cr/Al ratio value.

Figure 7 shows the mineralogical-geochemical cross-sections of chromitite-bearing zones of the Menzhinsky and Bolshoy Bashart deposits, which are typical of the Kraka peridotite–dunite–chromitite assemblages. The Cr# and Mg# values of Cr-spinel increase and decrease from peridotite to dunite and to chromitite, respectively. The Cr-spinel from "footwall" peridotite has higher Cr# values relatively to that

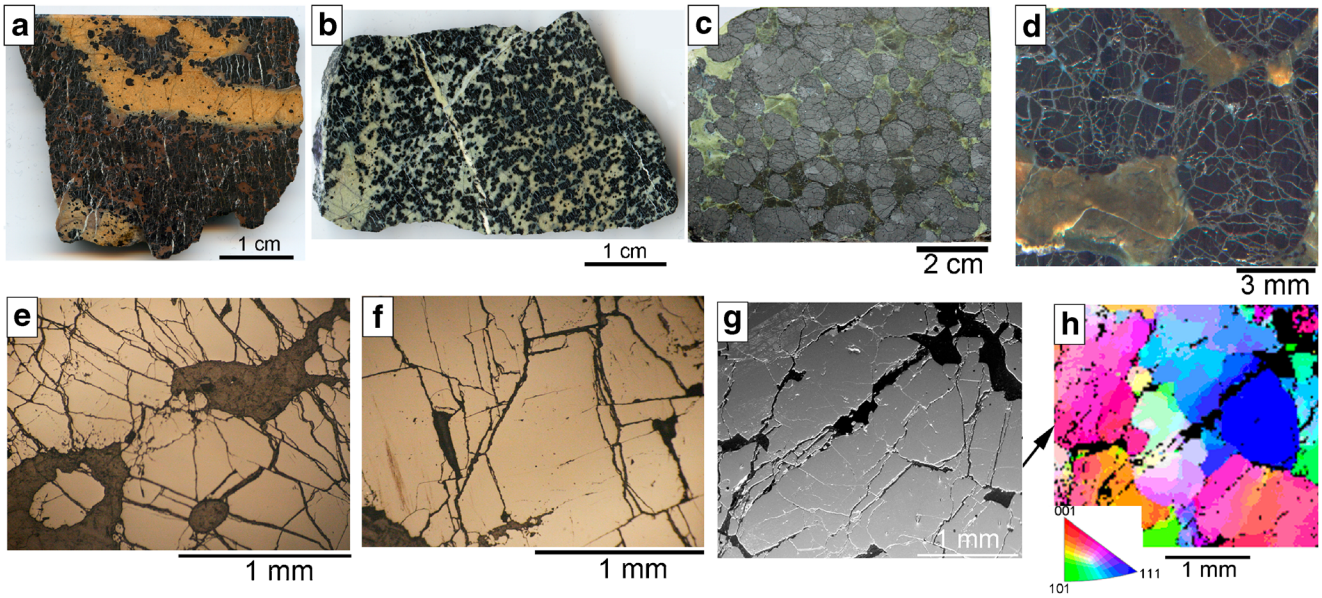

Fig. 5 Structural and textural features of densely disseminated, massive, and nodular chromitite from podiform deposits: **a** Massive chromitite band in serpentinized dunite from the Pridorozhnoe deposit. **b** Densely disseminated chromitite from the Laktybash deposit. **c–m** Chromitite from the no 33 deposit. **c–d** Nodular chromitite near massive ore. **e**, **f** Massive chromitite in reflected light: **e** Massive chromitite with strain-induced texture and "squeezed" interstitial silicates. **f** Massive chromite blocks shifted along the straight shear zones. **g** BSE images of massive chromitite. **h** The same area, EBSD image coded in inverted pole figures: there are deformed and recrystallized, growing grains

of "hanging wall" peridotite. Close to the ore bodies, Cr-spinel grains are characterized by a higher TiO_2 content, as well as V_2O_5 content in those from peridotite. The increase in Cr# value of Cr-spinel is accompanied by increasing Fo-content at constant NiO content in olivine.

Fabric of plastically deformed polycrystalline olivine

As was mentioned above, the olivine in peridotite and dunite of the mantle section of the Kraka ophiolites exhibits ubiquitous features of high-temperature plastic deformation, including kink-bands, polygonized structure of large crystals, and the presence of small recrystallized grains along the periphery and in internal parts of porphyroclasts with distorted crystal lattice. In outcrops and samples, foliation is typically identified by flattened tabular pyroxene grains and is nearly always parallel to banding. Lineation is traced by chains of Cr-spinel grains.

The features of olivine fabric are considered on example of the Maly Bashart deposit with abundant serpentinized spinel peridotite. The fabric diagrams for olivine from ore-hosting dunite and country rock spinel peridotite of the northern (YuK-2003), central (YuK-1982-1985), and southern (YuK-1978-1979) parts of the chromite-bearing zone are presented in ESM (Fig. S2). These diagrams indicate strong preferred orientation of optical indicatrix axes, but characterize different slip systems in olivine. The comparison with macrostructural elements of samples shows that the Ng axis ([100] direction) of olivine is always oriented close to the direction of plastic flow, locally, forming an acute angle. This causes a slip direction of [100] in olivine.

Peridotite exhibits simpler fabrics marked by obvious maxima of two other axes. The Nm axis ([001] direction) forms maxima along the foliation plane, whereas the Np axis ([010] direction) is perpendicular to this plane. This means that (010) is a slip plane and, correspondingly, the slip system is (010)[100]. The dunite is characterized by more complex distribution of [010] and [001] and typically forms girdles perpendicular to lineation. This fabric is interpreted as a result of intracrystalline gliding along the system {0kl}[100] (Carter 1976).

The (010)[100] slip system was active in peridotite of the northern part of the Maly Bashart area, whereas in dunite, it is replaced by multiple slip along the {0kl}100] system. In the central part of the chromite-bearing zone, peridotite close to the dunite body is characterized by flexural bends of banding and foliation. The peridotite exhibits different slip systems: single-component (010)[100] and complex slip system with (010)[100] and (001)[100] components. Multiple slips along the {0kl}[100] system is identified in dunite.

Flexural bend of structural elements and fabric pattern typical of the (010)[100] slip system is observed in peridotite with high proportions of pyroxene in the southern part of the zone, near the pinching out of the dunite body. More complex slip system is typical of sample YuK-1978-01. It is characterized by extension of the Nm axes

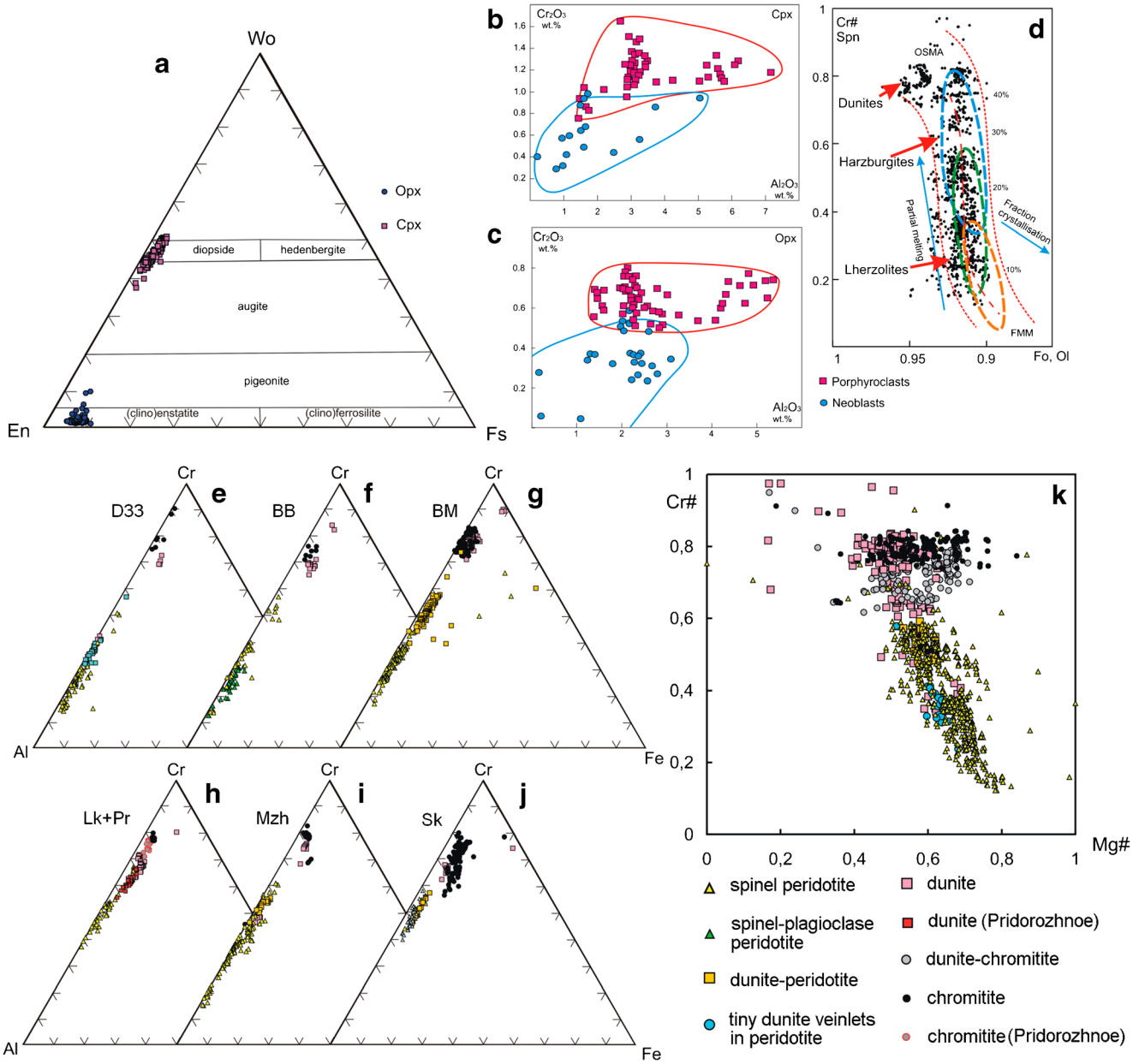

Fig. 6 Compositional variations of pyroxenes (**a–c**), olivine and chromite (**d–k**) from various areas of the Kraka massif. Deposits: D33, no 33; BB, Bolshoy Bashart; BM, Maly Bashart; Lk, Laktybash; Pr, Pridorozhnoe; Mzh, Menzhinsky; Sk, Saksey

into the girdle perpendicular to banding, similar to slip along {0kl}[100]; however, the Np axes form several maxima typical and atypical of this system. In both samples, the Ng axis maxima in olivine are deviate clockwise from the direction of lineation by a small angle (10–15°), which is characteristic of solid state flow under conditions of the dextral strike-slip fault. The fabric pattern in dunite is typical of multiple slips along {0kl}[100] as a result of axial deformation.

Similar features are registered in other chromitite deposits of the Kraka massifs: Bolshoy Bashart (samples YuK-1382, YuK-1386), Saksey (sample CK-1108), Laktybash (sample YuK-2014), Pridorozhnoe (sample YuK-2012), and no. 33 deposit (samples CK-103-2B, CK-103-4) (Fig. 8, Fig.S2). These examples demonstrate abundant plastic deformation of the upper mantle section in Kraka ophiolites. The higher rate of solid state flow is characteristic of dunite, the interlayers of which probably reflect zones of localization of solid state flow in the mantle.

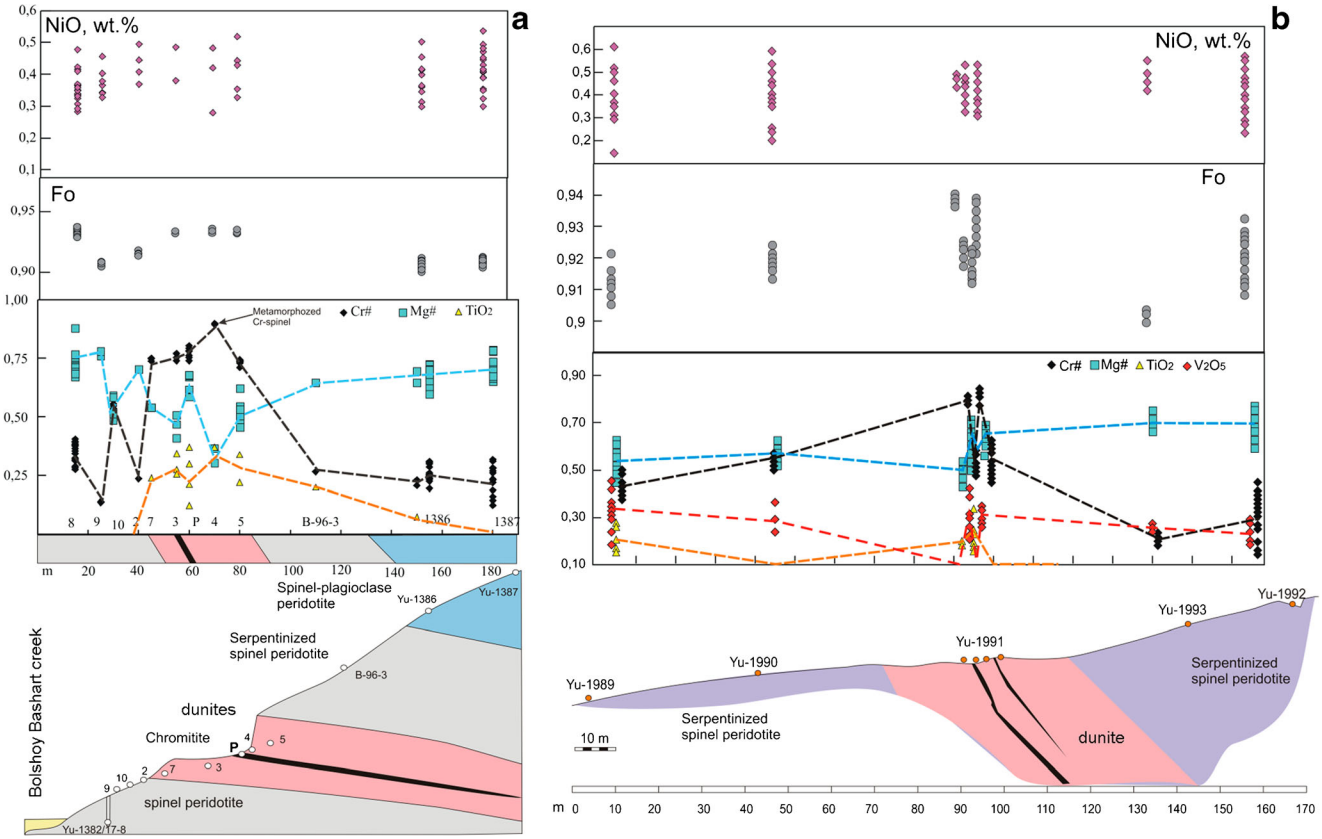

Fig. 7 Compositional variation of chromite along cross-sections of **a** Bolshoy Bashart and **b** Menzhinsky

Mineralogical and chemical alteration of ultramafic rocks induced by plastic deformation

Plastic deformation of mantle peridotite silicates is accompanied by structural, mineralogical, and geochemical alteration. In particular, plastically deformed olivine and orthopyroxene crystals host the smallest spinel grains.

The chromian spinel grains include several assemblage and morphology: (1) thin rods 5–10 μm long and 0.1–1.0 μm wide, located in deformed olivine crystals (Fig. 9), (2) elongated grains 10–50 μm long and 1–10 μm wide at the contacts of subgrains and olivine grains, locally, in form of branches from the larger Cr-spinel crystals (Fig. 9); (3) the smallest equiaxial crystals (few micrometers in diameter) in recrystallized zones of orthopyroxene (Fig. 10); (4) lamellae (1–50 μm long, 0.1–10 μm wide) in plastically deformed enstatite crystals, often in association with diopside and pargasite lamellae (Fig. 11; Fig.S3); and (5) the smallest equiaxial crystals (0.n–2 μm in diameter) in diopside lamellae and neoblasts, which formed during deformation of enstatite (Fig. 12).

Types 1 and 2 chromites are associated with each other or exhibit mutual gradational transitions. Figure 9 shows examples of various grains of these chromite types in peridotite olivine of no. 33 deposit, which underwent oxidation annealing at 850 °C (see above). The grains are oriented along [010] or [100]; in case of [100] orientation, they are almost perpendicular to kink-bands in olivine (Fig. 9c, d). Local thin Cr-spinel rods are confined to the low-angle boundaries in olivine and they are oriented across the boundary (Fig. 9g, h). The sigmoid morphology of grains is possibly related to their reorientation during matrix deformation (Fig. 9e, 9f). Figure 9i and j show that newly formed Cr-spinel crystals are in contact with small, recrystallized olivine fragments with lower density of dislocations, and separate them from the deformed olivine grain. The final result of this process is the formation of a continuous Cr-spinel rim around the olivine fragment.

Type 3 chromite grains are ubiquitous near plastically deformed enstatite crystals in association with enstatite II, diopside, and olivine neoblasts (Fig. 10). These Cr-spinel grains have an equiaxial morphology and size ranging from sub- to several microns. Their formation at the expense of recrystallization of primary enstatite is confirmed by significant depletion of enstatite neoblasts in Cr and Al in comparison with porphyroclasts.

Figure 10a-c show large kinked enstatite crystals, which contain lamellae of Na–Cr-rich pargasite in the (100) plane of host mineral, and flames of Na–Cr-rich pargasite directed

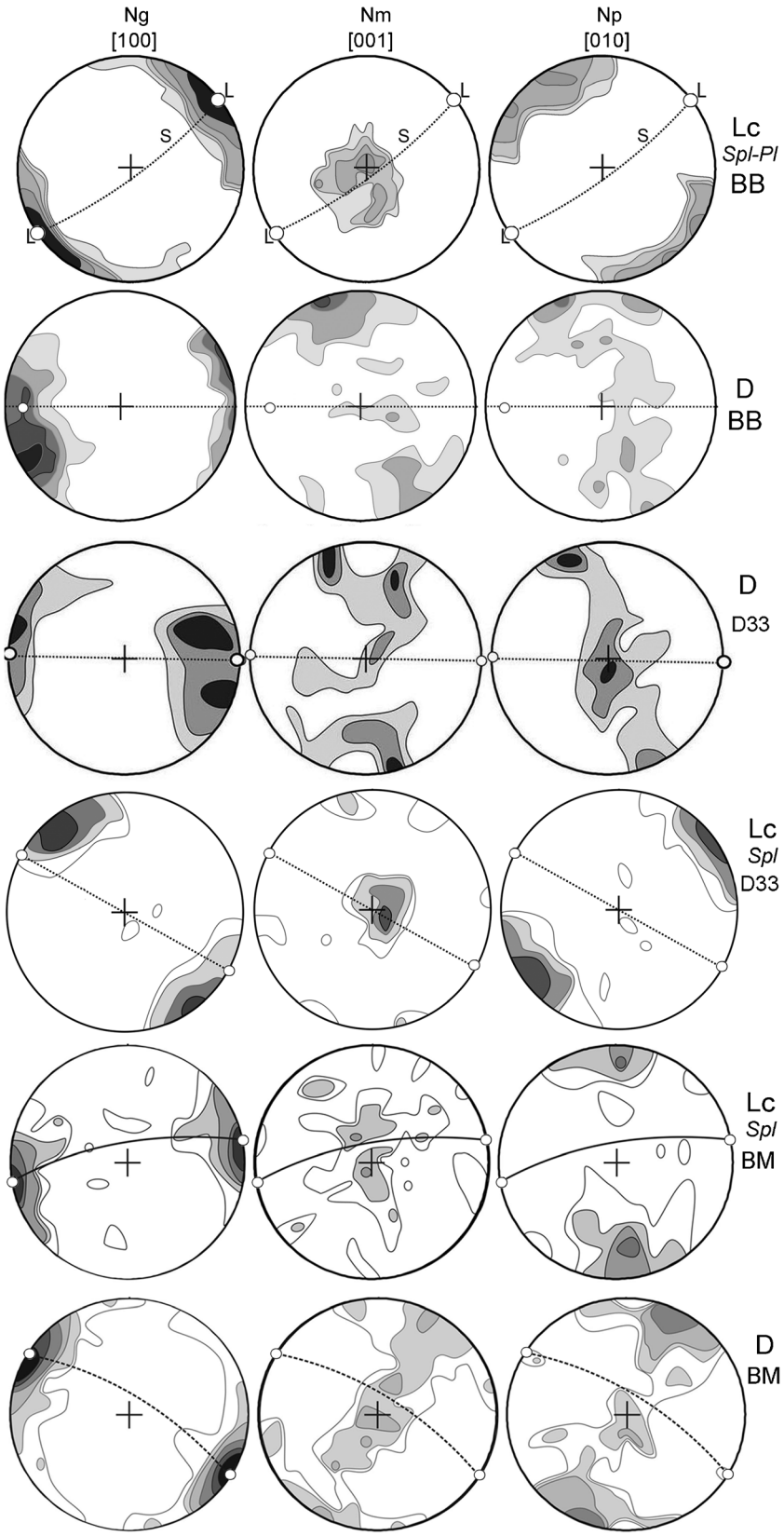

Fig. 8 Preferred crystallographic orientation of olivine grains in peridotite and dunite. Upper hemisphere of the Wulff net; 105–120 calculated points; circles, positions of lineation (L); lines, projections of foliation and banding (S); D, dunite, Lc Spl, spinel lherzolite; Lc Spl-Pl, spinel-plagioclase lherzolite; D33, deposit no. 33, BM, Maly Bashart, BB, Bolshoy Bashart

from kink-boundary to the recrystallization zone. The enstatite porphyroclast contains several olivine crystals stretched along the (100) plane of the host mineral. The recrystallization zones form in mostly distorted areas of the

lattice of primary enstatite (Fig. 10d). They contain numerous fine-grained equiaxial enstatite II and olivine Fa_{10} neoblasts with tiny Cr-spinel grains along their boundaries (Fig. 10e–j). Several vermicular segregations correspond to Na–Cr pargasite. They are elongated parallel to the foliation of the sample and are closely associated with numerous, tiny Cr-spinel grains and olivine neoblasts. Thus, we can conclude that the formation of pargasite segregations in enstatite is caused by deformation of the host mineral.

Type 4 chromite grains sporadically occur inside plastically deformed enstatite crystals but their study is hampered by their small crystal size. Sample CK-85/2 with numerous large lamellae was found in the central part of the Central Kraka block. Thin sections oriented in three mutually perpendicular planes, which coincide with (100), (110), and (001) crystallographic planes of enstatite, were prepared from CK-85/2 sample. All thin sections show ingrowths of diopside, Na–Cr-pargasite, and Cr-spinel in enstatite (Fig. 11). The (110) plane exhibits low-angle boundaries traced by vermicular pargasite grains, and large Cr-spinel crystals with no lamellae in vicinity. Apophyses of these Cr-spinel crystals are parallel to spinel lamellae in the (100) plane of enstatite. In Al–Cr–Fe^{+3} and Mg#–Cr# diagrams, the compositional fields of large Cr-spinel grains and lamellae are overlapped indicating their genetic similarity (Fig. S4).

Type 5 chromite grains are found in plastically deformed enstatite crystals from the Menzhinsky deposit peridotite. Plastic deformation of large orthopyroxene crystals is accompanied by the formation of diopside and pargasite lamellae in the (100) plane of the host mineral and neoblasts along their periphery and, rarely, in inner parts of crystals, which serve the nucleus for further growth of equiaxial neoblasts (Fig. 12a).

An important feature is related to the absence of lamellae near equiaxial neoblasts and their presence at a distance of 50–100 μm (Fig. 12b). Some neoblasts have complex structure, such as a neoblast shown in Fig. 12 which mostly consists of diopside transiting to pargasite and which contains the finest grained euhedral spinel inclusion ~ 1 μm. The neoblast is rimmed by a lamellae-free zone of relatively homogeneous structure.

The Cr-spinel grains in olivine crystals from spinel peridotite, which is adjacent to dunite or contains thin dunite veinlets, are generally characterized by lower Cr# value (0.1–0.4). High-Cr# (> 0.6) spinel rods occur in olivine from the Menzhinsky deposit dunite. The LA-ICP-MS analyses of olivine show a strong decrease in Al_2O_3 content and a small decrease in Cr_2O_3 content from peridotite to ore-hosting dunite (Saveliev and Artemyev 2021). In particular, olivine in distal spinel peridotite contains 100–400 ppm Al in contrast to that of dunite bodies from the Bolshoy Bashart and no. 33 deposits with 5–8 ppm Al. These features indicate strong depletion of Al in olivine during transition from peridotite to dunite that can be related to Al loss as a result of crystallization of new spinel crystals.

The Cr-spinel grains from plastically deformed orthopyroxene crystals and recrystallization zones have higher Cr_2O_3 content compared to those included in olivine. The Cr# values of Cr-spinel lamellae in enstatite (sample CK-85/2) and Cr-spinel from recrystallization of enstatite (sample CK-103-4) are 0.4–0.6 and 0.25–0.50, respectively. In adjacent, fine-grained spinel in olivine and enstatite (Fig. S3), the Cr# values differ almost by a factor of two, suggesting solid-state segregation of Al and Cr atoms from the crystal lattice of silicates.

Plastic deformation of pyroxene is accompanied by a regular change in its composition (Fig. 6b, c). The maximum Al_2O_3 and Cr_2O_3 contents are typical of large enstatite crystals, with a decrease in folded grains, whereas minimum concentrations are detected in small, recrystallized grains.

Discussion

Structural features of the deposits

The main structural features of all chromitite-bearing zones of the Kraka massifs include symmetric structural and mineralogical-geochemical zonation expressed in a synchronous change of several parameters from peripheral spinel peridotite to the central dunite body and chromitite (Chrt): (1) mineral assemblages (ol+opx+cpx+Cr-spl → ol+opx+Cr-spl → ol+Cr-spl → Chrt → ol+Cr-spl → ol+opx+Cr-spl → ol+opx+cpx+Cr-spl); (2) change in the slip system of olivine in peridotite from one-component (010)[100] to complex {0kl}[100] system in dunite; and (3) increasing Cr# value of spinel and Mg# value of olivine from peridotite to dunite and chromitite. These features are also typical of most podiform Cr deposits of ophiolite ultramafic rocks (e.g., Thayer 1964; Cassard et al. 1981; Chernyshov 1987; Shcherbakov 1990).

The ore zones always exhibit a gap in Cr# value of Cr-spinel from peridotite, from one hand, and chromitite and ore-hosting dunite from the other hand (Saveliev and Blinov 2017). The values of this gap depend on the deposit type and increase from tabular bodies composed of disseminated ore (Cr# value of < 0.05) to typical podiform massive chromitite (Cr# value of 0.08–0.12). Thus, understanding of the formation of chromitite requires identification of the relationship between plastic deformation, formation of dunite bodies, increasing amount of chromite, and changes in chemical composition of chromite.

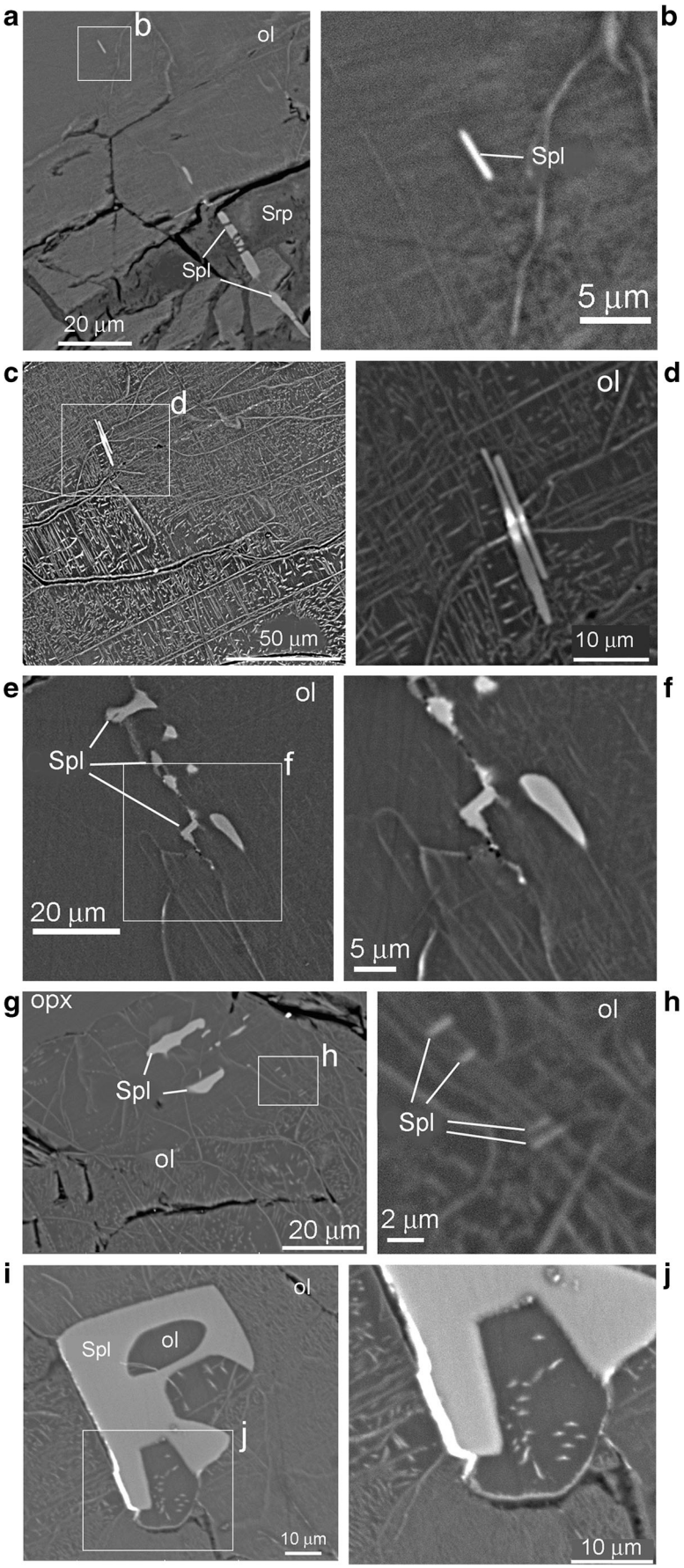

Fig. 9 Tiny chromite grains in deformed olivine crystals of peridotite of the no. 33 deposit. BSE images. The samples underwent oxidative annealing at 850 °C following method of (Kohlstedt et al. 1976). **a** Tiny chromite rod in the olivine volume continuing larger chromite grain. **b** Detail of the same rod. **c** Pair of chromite rods on subgrain boundaries conjunction and dislocation structure of host olivine. **d** Detailed area of the same pair of chromite rods. **e** Tiny chromite precipitation of various morphology and orientation close to the grain boundary of olivine grains. **f** S-shape chromite grain. **g** Small chromite grains among olivine neoblasts. **h** Detailed g-image: tiny chromite rods on the olivine grain boundary. **i** Chromite grain enclosing olivine fragments. **j** Olivine fragment with lower dislocation density. ol, olivine, opx, orthopyroxene, cpx, clinopyroxene, spl, Cr-spinel

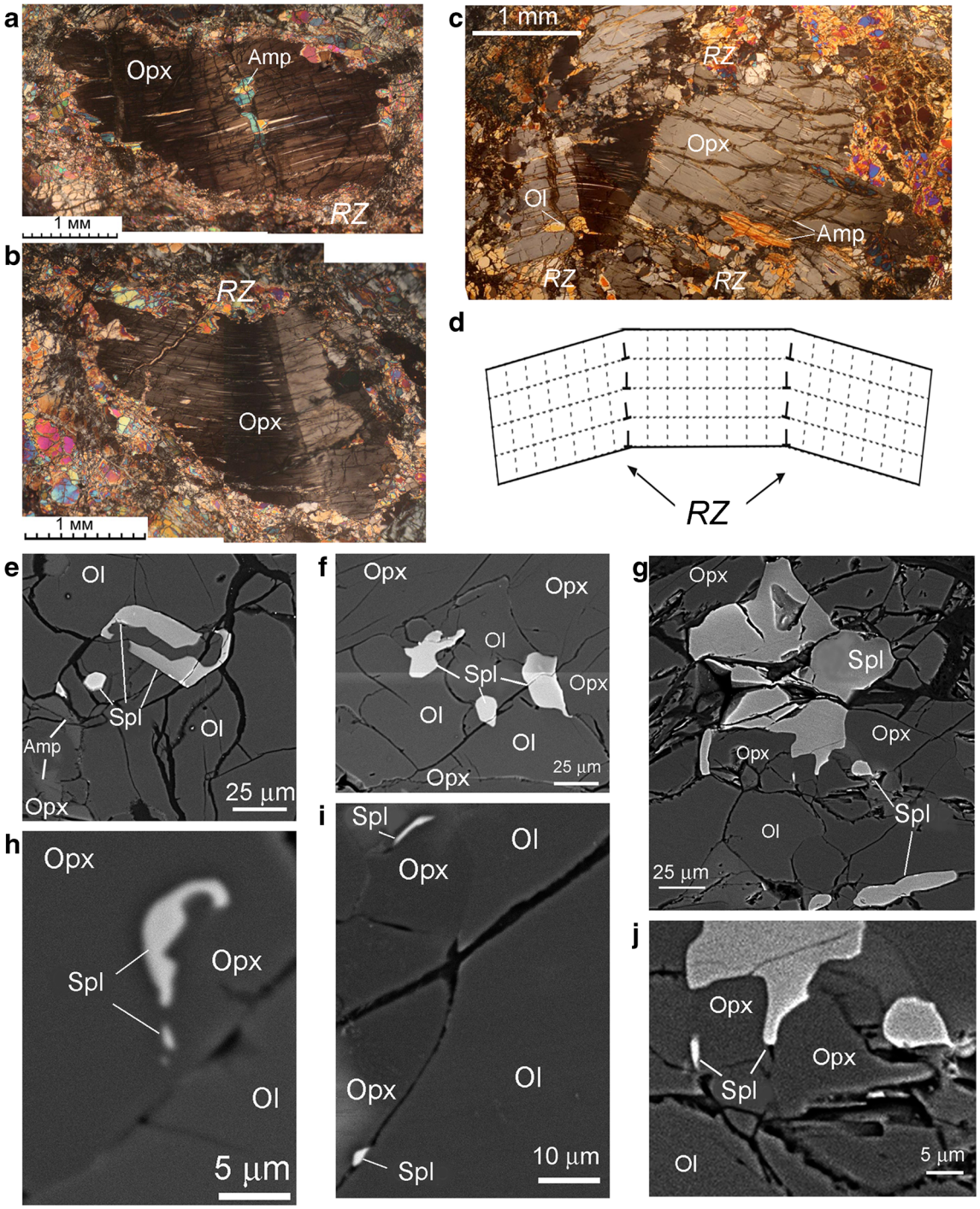

Fig. 10 Deformed enstatite crystals (**a**–**d**) and chromite grains in recrystallization zones (**e**–**j**). **a**–**c** Deformed enstatite crystals in peridotite from the no. 33 deposit (Central Kraka block) with kink-bands and pargasite and diopside lamellae along the glide planes and tilt walls. **d** Theoretical scheme of dislocation tilt wall in bended crystal relevant for interpretation of **a**–**c**; **e**, **h** Epitaxial chromite and olivine grains in plastically deformed peridotite. **f** Small chromite grains associated with olivine neoblasts near to the Opx porphyroclast. **g**, **j** chromite grains of various size among olivine and enstatite neoblasts. **i** Tiny chromite precipitation on the olivine/enstatite boundary. RZ, recrystallization zones in most distorted areas of the deformed enstatite. amp, amphibole (pargasite)

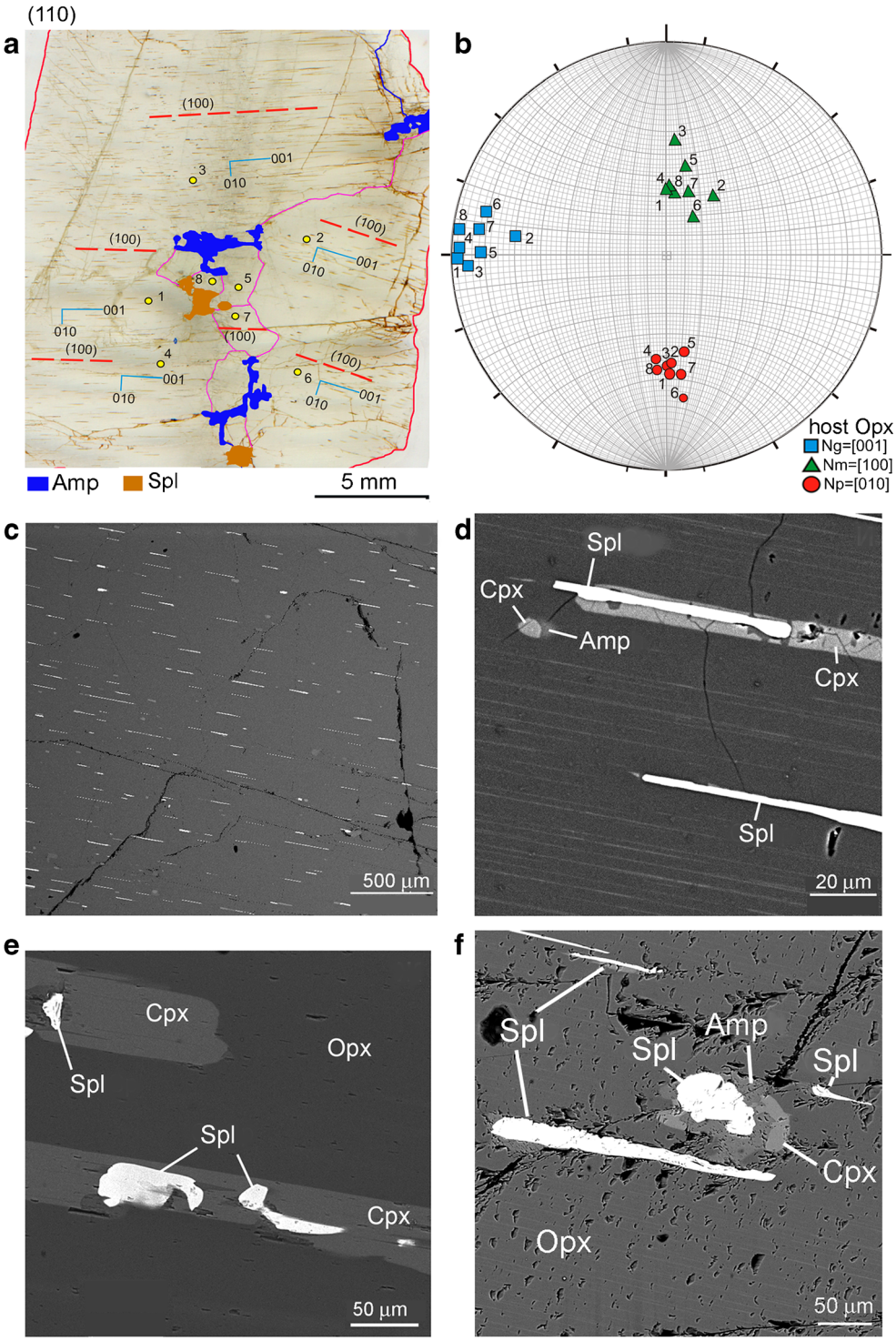

Fig. 11 Structure of plastically deformed crystals of enstatite (**a**, **b**) and chromite lamellae on the (100) plane of host mineral (**c**–**f**). **a** Schematic map of thin section CK-85/2 (central part of the Central Kraka block). **b** Projections of Opx axes on the upper hemisphere of Wulff net. **c**–**f** BSE images of studied Opx crystal. **c** General view of Opx lamellae structure. **d**-**e** Combined spinel-diopside lamellae and pargasite-diopside inclusion. **f** Chromite inclusions of various size and morphology

Plastic deformation of silicates and formation of chromian spinel crystals

Plastic deformation during uplift of the mantle material in decompression zones (Ringwood 1975; Anderson 1989) could have been a main trigger for trace element segregation in olivine and orthopyroxene grains. The uplift to less dense levels the Mantle is accompanied by decreasing capacity of the olivine cell to incorporate trace elements, in particular, Cr and Al (Dodd 1973; Zhang et al. 1999;

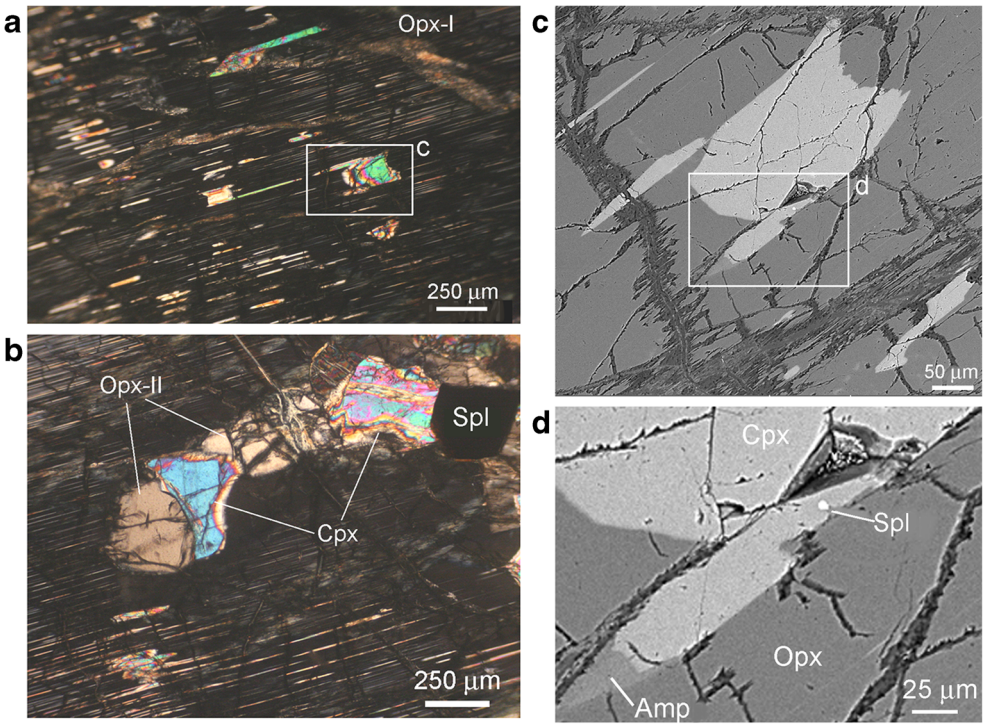

Fig. 12 Structure of plastically deformed crystals of enstatite with diopside lamellae and neoblasts. **a** General view of Opx porphyroclast with diopside lamellae and larger inclusions. **b** Neoblasts of chromite, diopside, and enstatite on the Opx porphyroclast margin. **c**–**d** Detailed images of diopside grain enclosing a tiny chromite precipitation. **a**, **b** Cross-polarized light; **c**, **d** BSE images; opx-I, large porphyroclast, opx-II, neoblasts

Franz and Wirth 2000). On the other hand, impurities are barriers for dislocation in olivine grains, promoting blocking and polygonization. The aggregates of rheologically stronger chromite yield strain, reducing mobility under solid state flow and resulting in spatial rearrangment of grains of two adjacent minerals.

The nucleation and growth of new chromite grains are similar to nucleation and growth of second phases during dynamic aging of solid solutions (Bunin and Baranov 1970; Novikov 1986). In metamorphic petrology, heterogeneous nucleation is a similar process (Stünitz 1998). Minimization of the grain boundary energy is a driving force for growing new grains and formation of euhedral crystals (Gorelik 1978).

In orthopyroxene, plastic deformation was accompanied by formation of stacking faults along the (100) slip plane, where lamellae of new phases (pargasite, diopside, Cr-spinel) formed from trace atoms segregated on structural defects (Van Duysen et al. 1985; Skrotzki 1994). Progressive deformation of the crystalline lattice led to intense recrystallization in most distorted sections and the formation of equiaxial neoblasts of enstatite II, diopside, pargasite, and Cr-spinel.

This can be a result of deformation-induced diffusion breakdown of enstatite followed by melting of newly formed amphibole (Saveliev et al. 2017). Friction melting caused by heat supply from deformed minerals on slip interfaces is one possible mechanism (Spray 1988, 1992). This process is sensitive to rheological properties of deformed minerals: in particular, enstatite and olivine are rheologically strong and weak phases, respectively (Carter 1976; Yamamoto et al. 2002, 2008; Karato 2008). Olivine is easily deformed, changing crystal morphology according to the stress field. Several slip systems can be active in olivine. In contrast, enstatite exhibits only one active (100)[001] slip system (McLaren and Etheridge 1976; Karato 2008; Jung 2017); thus, it accumulates deformation energy with increasing amount of defects of the crystalline structure. This energy causes crystal folding and increasing temperature activates diffusion processes in the grain (Spray 1988). For example, the amphibole-type defects could have formed first and the small amphibole grains could then melt due to lower melting point compared to the host mineral. Thus, simultaneous solid state flow and partial melting of rock-forming silicates is a potential scenario for Cr extraction from silicate phases.

The origin of dunite and chromitite

Numerous studies have attempted to explain the variable chemical composition of accessory and ore-forming Cr-spinels in ophiolite and oceanic ultramafic rocks (Ahmed 1984; Barnes and Roeder 2001). It was found that ophiolite Cr-spinels are characterized by a widely varying Cr/Al ratio, slightly distinct Mg/Fe ratio, and lower TiO_2 content

(Thayer 1964; Dickey 1975; Leblanc and Violette 1983). Most models for the formation of podiform deposits and host dunites are based on a leading role for melts and fluids generated by deeper mantle sources at middle ocean ridges (MORs) and/or supra-subduction zones (SSZ) settings (Roberts 1988; Ballhaus 1998). Earlier publications indicated the importance of fractional crystallization and deformation (Thayer 1964; Dickey 1975; Greenbaum 1977; Hock et al. 1986). Later studies were focused on identification of suitable conditions of crystallization of chromite as a result of chemical interaction of various melts and mixing (Lago et al. 1982; Ballhaus 1998; Matveev and Ballhaus 2002).

More recent studies consider mantle-melt interaction in various tectonic settings as a main reason of compositional variations of accessory and ore-forming chromite (Melcher et al. 1997; Morishita et al. 2006; Gonzalez-Jimenez et al. 2011; Kapsiotis et al. 2018; Kiseleva et al. 2020). These authors suggest that the high-Al and high-Cr spinels form in MOR and SSZ settings, respectively. If peridotite contains both chromite types, it formed in a MOR setting that evolved into a SSZ setting (Morishita et al. 2006; Gonzalez-Jimenez et al. 2011). If deposits with various chromite compositions are spatially separated in an ultramafic massif, they likely formed in different settings that were later combined tectonically (Melcher et al. 1997). The leading role of deep fluids in the formation of chromitite is based on observation of submicroscopic inclusions of "fluid-bearing" minerals (amphibole, phlogopite, chlorite, serpentine, carbon-containing phases) in chromite along with olivine, pyroxenes, and platinum group minerals typical of ultramafic rocks (Arai and Akizawa 2014; Pushkarev et al. 2015; Johan et al. 2017; El Dien et al. 2019).

The origin of podiform chromitite as a result of peridotite-melt interaction, magma mixing or fluid metasomatism, however, requires solution of the following problems: (1) the presence both of sharp and gradational contacts between dunite and peridotite, (2) the formation of massive chromitite lenses within relatively thin dunite envelopes, (3) folding of chromitite layers within dunite, and (4) co-existing pervasive plastic deformation with "primary igneous" poikilitic inclusions of olivine in chromite grains.

To solve these problems, we suggest an alternative model for the formation of dunite and chromitite based on the Kraka ophiolite massif. It is well known that the ophiolite chromitite deposits have widely variable amount of chromitite and size of deposits (Stoll 1958; Thayer 1964; Cassard et al. 1981; Hock and Friedrich 1985; Hock et al. 1986; Arai and Akizawa 2016). The geological and mineralogical features of most deposits are similar all over the world, in particular, the occurrence of a symmetric sequence "peridotite – dunite envelope – chromitite" (Thayer 1964; Cassard et al. 1981).

Thus, a transition from small streams of disseminated chromitite (initial stage) to large deposits of massive chromitite (final stage) is a result of the same ore-forming process, which can be interrupted at any stage. If the ore-forming process terminated at early stages, the ore and host rocks should exhibit its all features. For example, the formation of chromitite and dunite as a result of melt/mantle interaction (Kelemen et al. 1992, 1995; Zhou et al. 1994; Gonzalez-Jimenez et al. 2014) requires abundant relict pyroxene grains after dissolution along with crystallized reaction products. In case of magma-mixing models (Ballhaus 1998; Matveev and Ballhaus 2002), dunite and chromitite should contain all products of crystallization of mafic melts (e.g., plagioclase, clinopyroxene). In contrast, chromitite is typically enclosed in monomineral olivine aggregates (dunites), whereas mafic minerals (mostly, clinopyroxene) form thin veinlets and microinclusions.

The Kraka deposits and occurrences exhibit various termination stages of the ore-forming process. The earlier stages are recorded in most occurrences of the Apshak and Saksey-Klyuchevskaya areas with concordant disseminated chromitite. The next evolution stage of the ore-forming process is manifested in progressive segregation of chromite grains inside plastic flow at the Bolshoy Bashart, Maly Bashart, and Menzhinsky deposits. The final stage is observed at the no. 33 deposit with typical podiform massive chromitite.

In these areas, the ultramafic rocks show advanced deformation. The olivine grains have strong crystallographic fabric under high-temperature solid state flow. Our results are in agreement with experimental data and results of study of other ophiolite ultramafic rocks (Nicolas et al. 1971; Carter 1976; Poirier 1985; Goncharenko 1989; Shcherbakov 1990; Chernyshov 2001; Karato 2008; Jung 2017).

A thermodynamic model of redistribution of mineral phases in mantle solid state flow was developed by Saveliev and Fedoseev (2011, 2014, 2019) and Fedoseev (2016). It proposed that localization of plastic deformation occurs in rheologically weaker zones during mantle upwelling decompression under a dislocation creep regime. Because olivine is the softest phase of upper mantle rocks (Nicolas et al. 1971; Carter 1976; Yamamoto et al. 2002, 2008; Karato 2008), the solid state flow is more intense in dunite in comparison with peridotite; thus, the redistribution of mineral phases in dunite is more efficient.

The higher amount of chromite grains in dunite can be produced by (1) deformation-induced segregation of Al and Cr atoms from olivine and (2) deformation-induced breakdown of more rigid (in comparison with olivine) enstatite crystals, which can progressively be reduced in size during the solid state flow and finally dissolve into partial melt.

Under stress conditions, the composition of Cr-spinel changes from high-Al to high-Cr (Ozawa 1989; Suzuki et al. 2008; Saveliev and Blinov 2015; Shiryaev and Vakhrusheva 2017). The direct contact between dunite and peridotite with numerous newly formed chromite crystals is a critical zone for all these processes, because these crystals form as a result of deformation breakdown of pyroxene. Thus, pyroxene is sequentially reduced in amount and size and peridotite is transformed into dunite.

Finally, massive chromitites exhibit specific features, which can hardly be a result of simple crystallization from a melt or a result of chemical reactions, as suggested in the magma-mixing or melt-mantle interaction models, and require additional mechanisms of ore concentration. The structural features of massive chromitite aggregates indicate that they are the products of coalescent chromite grains under tectonic stresses, at high temperatures and pressures. The role of high-T creep in formation of podiform massive chromitite was identified using EBSD analysis (Ghosh et al. 2014, 2017; Satsukawa et al. 2015) as in this study.

A process similar to pressure sintering (Johnson 2012) is another candidate for the formation of massive chromitite, because sintering causes reorganization the grains, optimizing packing by maximizing the number of grain boundary contacts, increases the solubility, similar to pressure dissolution, where interstitial minerals (olivine, serpentine) in contact with more rigid chromite grains will be dissolved and removed to the lower pressure areas, and consequently favors transfer of the interstitial material away from the grain boundary contact areas, toward region of lower tensile stress. Pressure sintering is a variety of sintering, which combines compaction and sintering of the material at high homological temperature (0.5–0.8 T melting).

The structural features of massive chromitite aggregates are similar to those studied in polycrystalline tectonites (White and White 1981; Johnson 2012) including (1) thin tubular grain joints, (2) isolated voids, and (3) thin films of distorted crystal structure. Similar features are often observed in massive chromitite from ophiolites. These authors concluded that the grain structure formed as a result of intercrystalline mass transfer during deformation, wherein voids along the grain boundaries shorten the effective diffusion path. The high pressure and temperature, which is required for pressure sintering, could have been achieved in ophiolite chromitite at the expense of deformation energy in growing chromite aggregates inside dunite, because an increasing amount of chromite grains was unfavorable for the solid state flow inside a mobile dunite zone.

Conclusions

All chromitite deposits and occurrences of the Kraka ophiolite massif in the South Urals exhibit similar geological structure with chromitite hosted in dunite, widely variable thickness of the dunite envelopes, and no correlation between the size of ore bodies and the thickness of dunite. The disseminated fine-grained chromitite are separated from peridotite by thicker dunite bodies and massive podiform deposits are composed of coarse-grained chromitite and are surrounded by thin dunite envelope.

Peridotite, dunite, and chromitite of the Kraka deposits exhibit features of solid state flow during their formation in the upper mantle, preserved in high-PT plastic deformation in olivine and pyroxene and intensely folded chromitite in dunite. These features indicate that solid state flow always accompanied the formation of chromitite.

Plastic deformation of rock-forming silicates could have been a trigger for segregation of trace element atoms on structural defects in olivine and orthopyroxene that led to the decomposition of Opx. As a result of trace element segregation and recrystallization, orthopyroxene grains were reduced with formation of new Cr-spinels in areas of most intense plastic deformation, which were finally transformed into dunite.

The formation of dunite bodies and associated chromitite is related to the localization of deformation of rising mantle flows under decompression conditions. Dunite was the most rheologically weak zone exhibiting a focused solid state flow and effective separation of mineral phases (olivine and chromite).

The structural features of massive chromitite aggregates indicate that they formed by coalescence of ore grains under tectonic stresses at high temperatures and pressures. A process similar to pressure sintering is a possible scenario of their formation, which could have occurred during solid state mantle flow.

Supplementary Information The online version contains supplementary material available at https://doi.org/10.1007/s00126-021-01044-5.

Acknowledgements The author is grateful to Z. Vukmanovich, M. Fiorentini, W. Maier, and two anonymous reviewers and Editor-in-Chief Georges Beaudoin for their useful comments; I.A. Blinov (Institute of Mineralogy, SU FRC MB UB RAS, Miass), S.N. Sergeev, and I.I. Musabirov (Institute for Superplasticity of Metals, Ufa) for SEM studies; V.V. Shilovskikh (St. Petersburg State University, St. Petersburg) for EBSD analysis; and D.A. Artemyev (Institute of Mineralogy, SU FRC MB UB RAS, Miass) for LA-ICP-MS studies.

Funding This work was supported by the Government of the Russian Federation (projects nos. 0252–2017–0014 and 0246–2019–0078).

References

Ahmed Z (1984) Stratigraphic and textural variations in the chromite composition of the ophiolitic Sakhakot-Qila complex, Pakistan. Econ Geol 79:1334–1359

Anderson DL (1989) Theory of the Earth. Blackwell scientific publication, Boston, Oxford, London, Edinburgh, Melburn

Arai S, Akizawa N (2014) Precipitation and dissolution of chromite by hydrothermal solutions in the Oman ophiolite: new behavior of Cr and chromite. Am Mineral 99:28–34

Arai S, Miura M (2016) Formation and modification of chromitites in the mantle. Lithos 264:277–295

Ballhaus C (1998) Origin of the podiform chromite deposits by magma mingling. Earth Planet Sci Lett 156:185–193

Barnes S, Roeder P (2001) The range of spinel compositions in terrestrial mafic and ultramafic rocks. J Petrol 42:2279–2302. https://doi.org/10.1093/petrology/42.12.2279

Borisova AY, Ceuleneer G, Kamenetsky VS, Arai S, Béjina F, Abily B, Bindeman IN, Polvé M, De Parseval P, Aigouy T, Pokrovski GS (2012) A new view on the petrogenesis of the Oman ophiolite chromitites from microanalyses of chromite-hosted inclusions. J Petrol 53:2411–2440

Bunin KP, Baranov AA (1970) Metallography. Metallurgiya, Moscow (in Russian)

Carter NL (1976) Steady state flow of rocks. Rev Geophys Space Phys 14:301–360

Cassard D, Nicolas A, Rabinowitch M, Moutte J, Leblanc M, Prinzhoffer A (1981) Structural classification of chromite pods in Southern New Caledonia. Econ Geol 76:805–831

Chernyshov AI (2001) Ultramafic rocks (plastic flow, structural and petrostructural heterogeneity). Charodey, Tomsk (in Russian)

Coccomazi G, Grieco G, Tartarotti P, Bussolesi M, Zaccarini F, Crispini L, Oman Drilling Project Science Team (2020) The formation of dunite channels within harzburgite in the Wadi Tayin Massif, Oman Ophiolite: insights from compositional variability of Cr-Spinel and olivine in Holes BA1B and BA3A, Oman Drilling Project. Minerals 10:167. https://doi.org/10.3390/min10020167

Dickey JS (1975) A hypothesis of origin for podiform chromite deposits. Geochim Cosmochim Acta 39:1061–1075

Dodd RT (1973) Minor element abundances in olivines of the Sharps (H3) chondrite. Contrib Mineral Petrol 42:156–167

El Dien HG, Arai S, Doucet L-S, Li Z-X, Kil Y, Fougerouse D, Reddy SM, Saxey DW, Hamdy M (2019) Cr-spinel records metasomatism not petrogenesis of mantle rocks. Nat Commun 10:5103. https://doi.org/10.1038/s41467-019-13117-1

Fedoseev VB (2016) Stratification of two-phase monodisperse system in a laminar planar flow. J Exp Theor Phys 149(4):1057–1067. https://doi.org/10.1134/S1063776116040142

Franz L, Wirth R (2000) Spinel inclusions in olivine of peridotite xenoliths from TUBAF seamount (Bismarck Archipelago/Papua New Guinea): evidence for the thermal and tectonic evolution of the oceanic lithosphere. Contrib Mineral Petrol 140:283–295

Ghosh B, Ray J, Morishita T (2014) Grain-scale plastic deformation of chromite from podiform chromitite of the Naga-Manipur ophiolite belt, India: implication to mantle dynamics. Ore Geol Rev 56:199–208. https://doi.org/10.1016/j.oregeorev.2013.09.001

Ghosh B, Misra S, Morishita T (2017) Plastic deformation and post-deformation annealing in chromite: Mechanisms and implications. Am Mineral 102:216–226

Goncharenko AI (1989) Deformation and petrostructural evolution of Alpine-type ultramafic rocks. Tomsk University Publishing, Tomsk (in Russian)

Gonzalez-Jimenez JM, Proenza JA, Gervilla F, Melgarejo JC, Blanco-Moreno JA, Ruiz-Sanchez R, Griffin WL (2011) High-Cr and high-Al chromitites from the Sagua de Tanamo district, Mayari-Cristal ophiolitic massif (eastern Cuba): constrains on their origin from mineralogy and geochemistry of chromian spinel and platinum-group-elements. Lithos 125:101–121. https://doi.org/10.1016/j.lithos.2011.01.016

Gonzalez-Jimenez JM, Griffin WL, Proenza A, Gervilla F, O'Reilly SY, Akbulut M, Pearson NJ, Arai S (2014) Chromitites in ophiolites: how, where, when, why? Part II The crystallisation of chromitites. Lithos 189:148–158. https://doi.org/10.1016/j.lithos.2013.09.008

Gorelik SS (1978) Recrystallization of metals and alloys. Metallurgiya, Moscow (in Russian)

Greenbaum D (1977) The chromitiferous rocks of the Troodos ophiolite complex, Cyprus. Econ Geol 72:1175–1194

Hock M, Friedrich G (1985) Structural features of ophiolitic chromitites in the Zambales Range, Luzon, Philippines. Mineral Deposita 20:290–301

Hock M, Friedrich G, Plueger WL, Wichowski A (1986) Refractory- and metallurgical-type chromite ores, Zambales Ophiolite, Luzon, Philippines. Mineral Deposita 21:190–199

Jochum KP, Willbold M, Raczek I, Stoll B, Herwig K (2005) Chemical characterisation of the USGS Reference Glasses GSA-1G, GSC-1G, GSD-1G, GSE-1G, BCR-2G, BHVO-2G and BIR-1G using EPMA, ID-TIMS, ID-ICP-MS and LA-ICP-MS. Geostand Geoanal Res 29(3):285–302. https://doi.org/10.1111/j.1751-908X.2005.tb00901.x

Jochum KP, Weis U, Stoll B, Kuzmin D, Yang Q, Raczek I, Jacob DE, Stracke A, Birbaum K, Frick DA (2011) Determination of reference values for NIST SRM 610–617 glasses following ISO guidelines. Geostand Geoanal Res 35(4):397–429. https://doi.org/10.1111/j.1751-908X.2011.00120.x

Johan Z, Martin RF, Ettler V (2017) Fluids are bound to be involved in the formation of ophiolitic chromite deposits. Eur J Mineral 29:543–555

Johnson C (2012) Podiform chromite at Voskhod, Kazakhstan. Cardiff University, Dissertation

Jung H (2017) Crystal preferred orientations of olivine, orthopyroxene, serpentine, chlorite, and amphibole, and implications for seismic anisotropy in subduction zones: a review. Geosci J 21(6):985–1011. https://doi.org/10.1007/s12303-017-0045-1

Kapsiotis A, Rassios AE, Uysal I, Grieco G, Akmaz RM, Saka S, Bussolesi M (2018) Compositional fingerprints of chromian spinel from the refractory chrome ores of Metalleion, Othris (Greece): implications for metallogeny and deformation of chromitites within a "hot" oceanic fault zone. J Geochem Explor 185:14–32. https://doi.org/10.1016/j.gexplo.2017.11.003

Karato S-I (2008) Deformation of Earth materials. Cambridge University Press, An introduction to the rheology of solid Earth, 463 p

Kazantseva TT (1987) Allochthonous structures and an origin of the Uralian crust. Nauka, Moscow (in Russian)

Kelemen PB, Dick HJB, Quick JE (1992) Formation of harzburgite by pervasive melt/rock reaction in the upper mantle. Nature 358:635–641

Kelemen PB, Shimizu N, Salters VJM (1995) Extraction of mid-ocean-ridge basalt from the upwelling mantle by focused flow of melt in dunite channels. Nature 375:747–753

Kelemen PB, Hirth G, Shimizu N, Spiegelman M, Dick HJB (1997) A review of melt migration processes in the adiabatically upwelling mantle beneath oceanic spreading ridges. Philos Trans R Soc Lond Ser A 355:283–318

Kiseleva ON, Airiyants EV, Belyanin DK, Zhmodik SM (2020) Podiform chromitites and PGE mineralization in the Ulan-Sar'dag ophiolite (East Sayan, Russia). Minerals 10:141. https://doi.org/10.3390/min10020141

Kohlstedt DL, Goetze C, Durham WB, van der Sande JB (1976) A new technique for decorating dislocations in olivine. Science 191:1045–1046

Lago BL, Rabinowicz M, Nicolas A (1982) Podiform chromite ore bodies: a genetic model. J Petrol 23:103–125

Leblanc M, Ceuleneer G (1992) Chromite crystallization in a multicellular magma flow: evidence from a chromitite dike in the Oman ophiolite. Lithos 27:231–257

Leblanc M, Violette J-F (1983) Distribution of aluminium-rich and chromium-rich chromite pods in ophiolite peridotites. Econ Geol 78:293–301

Matveev S, Ballhaus C (2002) Role of water in the origin of podiform chromitite deposits. Earth Planet Sci Lett 203:235–243. https://doi.org/10.1016/S0012-821X(02)00860-9

McLaren AC, Etheridge MA (1976) A transmission electron microscope study of naturally deformed orthopyroxene. I. Slip mechanisms. Contrib Mineral Petrol 57:163–177

Melcher F, Grum W, Simon G, Thalhammer TV, Stumpfl EF (1997) Petrogenesis of the ophiolitic giant chromite deposits of Kempirsai, Kazakhstan: a study of solid and fluid inclusions in chromite. J Petrol 38:1419–1458

Morishita T, Andal ES, Arai S, Ishida Y (2006) Podiform chromitites in the lherzolite-dominant mantle section of the Isabela ophiolite, the Philippines. Island Arc 15:84–101. https://doi.org/10.1111/j.1440-1738.2006.00511.x

Nicolas A, Bouchez JL, Boudier F, Mercier JC (1971) Textures, structures and fabrics due to solid state flow in some European lherzolites. Tectonophysics 12:55–86

Novikov II (1986) Theory of thermal processing of metals. Metallurgiya, Moskow (in Russian)

Ozawa K (1989) Stress-induced Al–Cr zoning of spinel in deformed peridotites. Nature 338:141–144

Poirier J-P (1985) Creep of crystals. High-temperature deformation processes in metals, ceramics and minerals. Cambridge University Press. London

Puchkov VN (1997) Structure and geodynamics of the Uralian orogen. In Orogeny Through Time. Published by The Geological Society London. Ed. J.-P. Burg and M. Ford. P.201–236.

Puchkov VN (2002) Paleozoic evolution of the East European continental margin involved into the Urals. Mountain Building in the Uralides: Pangea to the Present. AGU Geophysics. Monogr. Ser. 132: 9–32.

Pushkarev EV, Kamenetsky VS, Morozova AV, Khiller VV, Glavatskykh SP, Rodemann T (2015) Ontogeny of ore Cr-spinel and composition of inclusions as indicators of the pneumatolytic–hydrothermal origin of PGM-bearing chromitites from Kondyor massif, the Aldan Shield. Geol Ore Depos 57:352–380

Ringwood AE (1975) Composition and structure of the Earth's mantle. McGraw-Hill, New York

Rost F (1959) Probleme ultrabasischer Gesteine und ihrer Lagerstatten. Freiberger Forschungshefte, Berlin

Satsukawa T, Piazolo S, González-Jiménez J-M, Colás V, Griffin WL, O'Reilly SY, Gervilla F, Fanlo I, Kerestedjian TN (2015) Fluid-present deformation aids chemical modification of chromite: Insights from chromites from Golyamo Kamenyane, SE Bulgaria. Lithos 228–229:78–89. https://doi.org/10.1016/j.lithos.2015.04.020

Saveliev DE, Artemyev DA (2021) Geochemical features of plastically deformed olivine from ophiolite peridotites and dunites of Kraka massifs (the Southern Urals). Zapiski RMO 150(1) (in press) (in Russian)

Saveliev DE, Blinov IA (2015) Syndeformation chrome spinel exsolutions in plastically deformed olivine aggregates (Kraka ophiolite, South Urals). Vestnik Permskogo Universiteta. Geologiya 4(29): 45–69 (in Russian). doi: 10.17072/psu.geol.29.44

Saveliev DE, Blinov IA (2017) Compositional variations of chrome spinels in ore-bearing zones of the Kraka ophiolite and origin of chromitite. Vestnik Permskogo universiteta. Geologiya 16(2):130–156. DOI: 10.17072/psu.geol.16.2.130

Saveliev DE, Fedoseev VB (2011) Segregation mechanism of formation of chromitites in ultramafic rocks of fold belts. Rudy Metally 5:35–42 (in Russian)

Saveliev DE, Fedoseev VB (2014) Plastic flow and rheomorphic differentiation of mantle ultramaflc rocks. Vestnik Permskogo Universiteta. Geologiya 4(25):22-41 (in Russian) doi: 10.17072/psu.geol.25.22

Saveliev DE, Fedoseev VB (2019) Solid-state redistribution of mineral particles in the upwelling mantle flow as a mechanism of chromite concentration in the ophiolite ultramafic rocks (by the example of Kraka ophiolite, the Southern Urals). Georesources 21(1):31–46. https://doi.org/10.18599/grs.2019.1.2-10

Saveliev DE, Snachev VI, Savelieva EN, Bazhin EA (2008) Geology, petrogeochemistry, and chromite content of gabbro-ultramafic massifs of the South Urals. DizaynPoligrafServis, Ufa (in Russian)

Saveliev DE, Puchkov VN, Sergeev SN, Musabirov II (2017) Deformation-induced decomposition of enstatite in mantle peridotite and its role in partial melting and chromite ore formation. Dokl Earth Sci 476:1058–1061

Savelieva GN (1987) Gabbro-ultramafic complexes of the Uralian ophiolites and their analogs in the present-day oceanic crust. Nauka, Moscow (in Russian)

Senchenko GS (1976) Fold structures of the South Urals. Nauka, Moscow (in Russian)

Shcherbakov SA (1990) Plastic deformations of ultramafic rock of the Uralian ophiolite association. Nauka, Moscow (in Russian)

Shiryaev PB, Vakhrusheva NV (2017) Chemical zoning of spinels and olivines from chromitites and the enclosing ultramafites of the Rai-Iz massif, Tsentralnoe deposit (the Polar Urals). News of the Ural State Mining University, 4:29–35. DOI 10.21440/2307-2091-2017-4-29-35

Shiryaev PB, Vakhrusheva NV (2018) The redox state of chromitites from the Yambotyvissky area (Voikar-Syninsky massif, Polar Urals). News Ural State Min Univ 4(52):33–40. https://doi.org/10.21440/2307-2091-2018-4-33-40

Skrotzki W (1994) Defect structure and deformation mechanisms in naturally deformed augite and enstatite. Tectonophysics 229:43–68

Spiegelman M, Kelemen PB, Aharonov E (2001) Causes and consequences of flox organization during melt transport: the reaction infiltration instability in compactible media. J Geophys Res 106: 2061–2077. https://doi.org/10.1029/2000JB900240

Spray JG (1988) Generation and crystallization of an amphibolite shear melt: an investigation using radial friction welding apparatus. Contrib Mineral Petrol 99:464–475

Spray JG (1992) A physical basis for the frictional melting of some rock-forming minerals. Tectonophysics 204:205–221

Stoll WC (1958) Geology and petrology of the Masinloc chromite deposit, Zambales, Luzon, Philippine islands. Bull Geol Soc Am 89:410–448

Stünitz H (1998) Syndeformational recrystallization ± dynamic or compositionally induced? Contrib Mineral Petrol 131:219–236

Suzuki AM, Yasuda A, Ozawa K (2008) Cr and Al diffusion in chromite spinel: experimental determination and its implication for diffusion creep. Phys Chem Miner 35:433–445

Thayer TP (1964) Principal features and origin of podiform chromite deposits, and some observations on the Guleman-Soridag District, Turkey. Econ Geol 59:1497–1524

Van Duysen JC, Doukhan N, Doukhan JC (1985) Transmission electron micro-scope study of dislocations in orthopyroxene $(Mg, Fe)_2Si_2O_6$. Phys Chem Miner 12:39–44

White JC, White SH (1981) The structure of grain boundaries in tectonites. Tectonophysics 78:613–628

Yamamoto J, Kagi H, Kaneoka I, Lai Y, Prikhod'ko VS, Arai S (2002) Fossil pressures of fluid inclusions in mantle xenoliths exhibiting rheology of mantle minerals: implications for the geobarometry of

mantle minerals using micro Raman spectroscopy. Earth Planet Sci Lett 198:511–519. https://doi.org/10.1016/S0012-821X(02)00528-9

Yamamoto J, Ando J, Kagi H, Inoue T, Yamada A, Yamazaki D, Irifune T (2008) In situ strength measurements on natural upper-mantle minerals. Phys Chem Miner 35:249–257. https://doi.org/10.1007/s00269-008-0218-6

Zagrtdenov NR, Ceuleneer G, Rospabe M, Borisova AY, Toplis M, Benoit M, Abily B (2018) Anatomy of a chromitite dyke in the mantle/crust transition zone of the Oman ophiolite. Lithos 312–313:343–357. https://doi.org/10.1016/j.lithos.2018.05.012

Zhang RY, Shu JF, Mao HK, Liou JG (1999) Magnetite lamellae in olivine and clinohumite from Dabie UHP ultramafic rocks, central China. Am Mineral 84:564–569

Zhou MF, Robinson PT, Bai WJ (1994) Formation of podiform chromites by melt/rock interaction in the upper mantle. Mineral Deposita 29:98–101

Zhou M-F, Robinson PT, Malpas J, Li Z (1996) Podiform chromitites in the Luobusa Ophiolite (Southern Tibet): implications for melt-rock interaction and chromite segregation in the upper mantle. J Petrol 37:3–21

Zhou M-F, Robinson PT, Malpas J, Aitchison J, Sun M, Bai WJ, Hu XF, Yang JS (2001) Melt/rock interaction and melt evolution in the Sartohay high-Al chromite deposit of the Dalabute ophiolite (NW China). J Asian Earth Sci 19:519–536